The near-tip region of a fluid-driven fracture propagating in a permeable elastic solid

By E. DETOURNAY[1] AND D. I. GARAGASH[2]

[1]Department of Civil Engineering, University of Minnesota, Minneapolis, MN 55455, USA
detou001@umn.edu

[2]Department of Civil and Environmental Engineering, Clarkson University,
Potsdam, NY 13699-5710, USA
garagash@clarkson.edu

This paper is concerned with an analysis of the near-tip region of a fluid-driven fracture propagating in a permeable saturated rock. It focuses on the calculation of the pore fluid pressure in the tip cavity, the region corresponding to the lag between the front of the fracturing fluid and the fracture tip. In contrast to impermeable rocks where the tip cavity can be considered to be at zero pressure, the fluid pressure in the tip cavity is here unknown and not uniform as exchange of pore fluid between the cavity and the porous medium and flow of pore fluid within the cavity is taking place. Solution of the fluid pressure in the tip region requires therefore simultaneous consideration of fracture mechanics (for the aperture of the tip cavity), diffusion theory for the movement of fluid within the porous medium, and viscous flow along the crack. Construction of such a solution within the framework of some simplifying assumptions is the main objective of this paper. It is shown that the problem depends, in general, upon two numbers with the meaning of a permeability and a propagation velocity. For the asymptotic case of large propagation speed, these two numbers merge into a single parameter, while the solution becomes independent of the propagation velocity in the limit of small velocity. The particular case of large velocity is solved analytically, while both the general and the small velocity cases are computed numerically but with different techniques. The paper concludes with a comprehensive analysis of numerical results.

1. Introduction

Fractures that are driven by a viscous fluid represent a particular class of tensile fractures. This mode of tensile fracture propagation takes place in hydraulic fracturing, a method widely used in the petroleum industry to stimulate underground reservoirs of hydrocarbons, in the formation of intrusive dykes in the earth's crust, and in the transport of magma in the lithosphere by means of fractures. The range of parameters characterizing these problems could be widely different, however. For example, dykes have typically a length L of order 10^3 to 10^4 m, a width w of order 1 to 10 m, with the viscosity μ_f of the basalts and rhyolites during formation of the dykes estimated to be of the order of 10 to 10^2 Pa s and 10^5 to 10^8 Pa s, respectively. In contrast, hydraulic fractures driven by injection of a viscous fluid in a wellbore would be described by L in the range of 10 to 10^2 m, w of order 10^{-3} to 10^{-2} m, and μ_f varying from 10^{-1} to 1 Pa s. Furthermore, the permeability of the host rock could vary over a large range of magnitudes, from 10^{-9} to 1 Darcy.

Following the seminal paper of Kristianovic & Zheltov (1955), numerous publications have tackled the problem of fluid-driven fractures with various degrees of approximation (see e.g. Barenblatt 1962; Perkins & Kern 1961; Nordgren 1972; Abé, Mura & Keer 1976; Geerstma & Haafkens 1979; Spence & Sharp 1985; Spence & Turcotte 1985; Lister 1990; Rubin 1995; Papanastasiou 1997; Carbonell, Desroches & Detournay 1999; Garagash 2000; Savitski & Detournay 2001; Garagash & Detournay 2002; Adachi & Detournay 2002; Adachi, Detournay & Carbonell 2003; for some of the more analytical contributions). The main difficulty in solving such a problem arises from having to deal simultaneously with a non-local relationship between the fracture opening and the fluid pressure, a nonlinear equation describing the flow of fluid with the crack, and, in the case of a permeable medium, a time-dependent equation that governs the exchange of fluid between the fracture and the rock. Furthermore, it has also recently been recognized (Spence & Sharp 1985; Lister 1990; Desroches *et al.* 1994; Garagash & Detournay 2000; Detournay, Adachi & Garagash 2002) that the handling of the region near the fracture tip poses special challenges, owing to the nature of the boundary conditions in the tip region and a rapid change of the fluid pressure, which both affect the overall solution.

In an impermeable medium, the structure of the near-tip solution is now understood, at least within the range of applicability of linear elastic fracture mechanics and lubrication theory. This solution is characterized by the existence of a lag between the fracturing fluid and the crack tip, as a weak negative singularity in the fluid pressure would otherwise exist if the fluid were allowed to reach the fracture tip. In impermeable rock, the tip cavity is filled with fluid vapours or by exsolved volatiles which can generally be considered to be at zero pressure (as the vapour pressure can usually be assumed to be negligible compared to the reference *in situ* stress). The size of the lag between the fracturing fluid front and the advancing fracture tip is *a priori* unknown and part of the solution (Lister 1990; Garagash & Detournay 2000). At intermediate distances from the tip (i.e. at distances large compared to the tip cavity size, yet small compared with the overall dimension of the fracture – assuming that such a range exists), the fluid pressure and fracture opening is given by an intermediate asymptote (Garagash & Detournay 2000). This intermediate asymptote is a singular solution, constructed by assuming that the fluid reaches the tip of a fracture propagating in a zero toughness solid (Spence & Sharp 1985; Lister 1990; Desroches *et al.* 1994). Existence of this intermediate region, which is characterized by large fluid pressure gradient and large dissipation of energy in the fluid, actually corresponds to a set of conditions for which the global solution (and in particular the fracture length, the fluid pressure and crack opening at the fracture inlet) is insensitive to the details of the tip solution.

This paper is concerned with the near-tip analysis of a fluid-driven fracture propagating in a permeable saturated rock. It focuses on the calculation of the fluid pressure in the tip cavity, which is filled by pore fluid. As in impermeable rocks, the front of the fracturing fluid lags behind the fracture tip (as it would otherwise cause a weak singularity in the fracturing fluid pressure). However, in contrast to impermeable rocks where the tip cavity can be considered to be at zero pressure, the fluid pressure in the tip cavity is now unknown and furthermore not uniform, as exchange of pore fluid between the cavity and the porous medium, and flow of pore fluid within the cavity is taking place. Indeed, pore fluid is drawn in, by suction, at the tip of the advancing fracture, and is reinjected to the porous medium behind the tip, near the interface between the two fluids. (Pore fluid must necessarily be returning to the porous rock from the cavity, as it would otherwise cause an increase of the lag

between the fracturing fluid and the tip of the fracture, which is clearly inconsistent with the assumption of stationarity.)

Solution of the pressure field within the cavity requires therefore simultaneous consideration of fracture mechanics (for the aperture of the tip cavity), diffusion theory for the movement of fluid within the porous medium, and viscous flow along the crack. Construction of such a solution within the framework of some simplifying assumptions is the main objective of this paper. This solution should be viewed as providing the appropriate tip conditions when considering either the large-scale problem or at least the intermediate scale which could be treated by analysing the propagation of a semi-infinite fracture.

Several authors (among them Geerstma & de Klerk 1969; Zazovskyi & Panko 1978; Nilson 1988; Detournay, Cheng & Mclennan 1990; Rubin 1993; Gordeyev 1993; Lenoach 1995) have considered the propagation of a fluid-driven fracture in permeable rocks. However, the tip cavity, which is the focus of this paper, appears to have been analysed only by Rubin (1993) in the context of permeable rocks. In that paper, the fluid pressure in the tip cavity is assumed to be uniform and given by the undrained pore pressure computed in the rock at the tip of the advancing fracture, assuming a Barenblatt-type process zone. Also, the exchange of fluid flow between the cavity and the rock is taken to be 'unidirectional', with the fluid flowing into the tip cavity.

This paper is organized as follows. After defining the specific problem to be solved here, the governing equations are presented. The problem is then reformulated in dimensionless form, following the introduction of lengthscales and characteristic pressure and velocity. It is shown that the problem depends in general upon two dimensionless numbers with the meaning of a permeability and a propagation velocity. However, these two numbers merge into a single parameter for the asymptotic case of large propagation speed, while the solution becomes independent of the propagation velocity, in the limit of small velocity. The particular case of large velocity is solved analytically, whereas both the general and the small velocity case are computed numerically but with different techniques. Finally, numerical results are presented and discussed.

2. Problem formulation

2.1. *Problem definition and assumptions*

The problem of the tip of a fluid-driven fracture, propagating at a speed V in a permeable rock with a far-field pore pressure p_o, is sketched in figure 1. The tip region is characterized by the existence of a cavity of length λ which separates the front of the fracturing fluid from the tip of the advancing fracture. This cavity is filled by pore fluid which has been sucked in from the permeable saturated rock. Fluid is circulating between the cavity and the rock. The governing equations are formulated in the moving coordinates system (x, y), with the origin centred on the crack tip and with the x-axis pointing inside the fracture, see figure 1. A fixed coordinates system (X, Y) is also introduced: $x = X + Vt$ and $y = Y$.

The main objective of this analysis is to calculate the fluid pressure distribution in the tip cavity (in particular the pressure at the interface between the two fluids) as a function of the tip velocity V, the cavity length λ, the far-field pore pressure p_o and several other mechanical parameters characterizing the fluid and the rock.

The analysis is performed under the following assumptions.

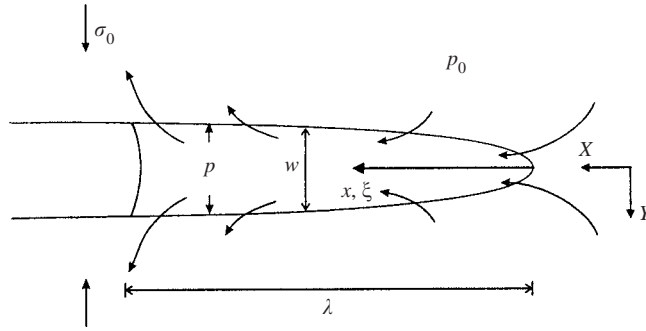(i) The fracture propagates in a permeable linear elastic solid.

FIGURE 1. Fluid-driven crack with the near-tip cavity.

(ii) The problem is stationary, i.e. the tip velocity V and the tip cavity length λ remains constant during propagation.

(iii) The problem of the tip region is treated as two-dimensional (plane strain), which is justifiable under the conditions that the length of the cavity is much smaller than the radius of curvature of the fracture edge.

(iv) The cavity lies entirely within the region dominated by the singularity of linear elastic fracture mechanics; this implies that the aperture of the tip cavity follows a linear square root variation from the tip.

(v) The pore pressure field in the permeable rock is governed by the homogeneous diffusion equation. Thus, the poroelastic coupling between solid deformation and pore fluid diffusion, as is accounted for in the theory of poroelasticity (Biot 1941; Rice & Cleary 1976; Detournay & Cheng 1993) and manifested by a inhomogeneous term in the pore pressure diffusion equation, is neglected here.

(vi) The pore pressure perturbation associated with leak-off of the fracturing fluid behind the tip cavity is not influencing the circulation of pore fluid in and out of the tip cavity. In other words, the fracture wall behind the cavity tip is treated as impermeable, from the point of view of modelling the diffusion of pore pressure in the vicinity of the tip region. The assumption of an impermeable fracture wall behind the tip cavity is an excellent approximation under conditions where the depth of penetration of the fracturing fluid in the fracture wall, in the region where the pore pressure is perturbed by the tip cavity, is indeed very small compared to the lengthscales characterizing the tip problem. This assumption can generally be justified by noting that the viscosity of the fracturing fluid is typically at least two orders of magnitude larger than that of the pore fluid in the context of the stimulation of oil wells (not accounting for the 'cake-building' property of these fluids) and many more orders of magnitude more in the case of magma-driven fractures (dykes).

(vii) The flow of fluid within the tip cavity is modelled by the lubrication equations, modified to take into account exchange of pore fluid between the tip cavity and the permeable rock. The fluid in the cavity is treated as incompressible.

(viii) A sharp interface between the pore fluid and the fracturing fluid exists.

2.2. *Governing equations*

The governing equations involve the following main quantities: the crack opening $w(x)$, the fluid pressure in the fracture $p(x)$, the flux discontinuity across the fracture $g(x)$, and the flow rate inside the crack $q(x)$ per unit extent of the crack in the direction perpendicular to the (X, Y)-plane. These quantities do not depend on time t,

in view of the stationarity assumption; also they need to be defined only on the interval $0 < x < \lambda$, corresponding to the tip cavity. The flux discontinuity $g(x)$ is taken as positive if fluid is leaving the fracture (g can thus be interpreted as a source density outside the fracture) and $q(x)$ is an 'absolute' flow rate defined with respect to the fixed coordinate system (X, Y); $q(x)$ is positive if the flux is in the same direction as the x-axis (or X-axis).

The formulation of this problem also requires us to introduce the pore pressure field $p(x, y)$; the field $p(x, y)$ takes the constant value p_o at infinity and is equal to the fluid pressure in the tip cavity, i.e. $p(x, 0) = p(x)$, $0 \leqslant x \leqslant \lambda$ (use of different symbols to differentiate between the fluid pressure in the fracture and the interstitial fluid pressure in the porous medium is not deemed necessary).

The mathematical model consists of equations from linear elastic fracture mechanics (LEFM), diffusion theory and lubrication theory, which describe the three coupled processes: fracturing of the medium, fluid flow inside the tip cavity and diffusion of pore fluid in the surrounding porous medium, respectively.

2.2.1. *Fracture propagation*

Linear elastic fracture mechanics (LEFM) provides a description of the first process. Within the framework of LEFM, the Griffith (1921) energy criterion of fracture propagation can be expressed in terms of the strength of the inverse square root stress singularity arising at the tip (Irwin 1957). The strength of this singularity, denoted as the stress intensity factor K_I (with dimension $[K_I] = FL^{-3/2}$), is an integral measure of the loading on the body containing the crack. The condition of continuous quasi-static propagation of a fracture in mobile equilibrium can then be expressed as

$$K_I = K_{Ic}, \tag{2.1}$$

where K_{Ic} is the fracture toughness, a material parameter which is related to the Griffith surface energy. An integral relation between the crack aperture w and the net loading on the fracture is provided by LEFM. The near-tip asymptote of this relation can be expressed, however, simply in terms of K_I (Rice 1968),

$$w = \frac{4K_I}{E'} \left(\frac{2x}{\pi} \right)^{1/2}, \tag{2.2}$$

where E' is the so-called plane strain modulus, which is related to Young's modulus E and Poisson ratio ν by $E' = E/(1 - \nu^2)$. Since it is assumed that the tip cavity lies entirely within the region dominated by the LEFM singularity, it follows from (2.1) and (2.2) that the aperture of the tip cavity is known.

2.2.2. *Lubrication flow in the cavity*

The pore fluid flow in the tip cavity ($0 < x < \lambda$, $y = 0$) is assumed to be governed by the lubrication theory for an incompressible fluid (Batchelor 1967). The lubrication equations in the fixed coordinate system consist of the one-dimensional continuity equation

$$\frac{\partial w}{\partial t} + \frac{\partial q}{\partial X} = -g, \tag{2.3}$$

and Poiseuille law

$$q = -\frac{w^3}{12\mu} \frac{\partial p}{\partial X}, \tag{2.4}$$

where μ is the dynamic viscosity of the pore fluid. The right-hand side in (2.3) accounts for fluid exchange between the cavity and the porous rock. Under the assumption of stationarity, lubrication equations (2.3)–(2.4) in the moving coordinate system are given by

$$V\frac{\mathrm{d}w}{\mathrm{d}x} + \frac{\mathrm{d}q}{\mathrm{d}x} = -g, \qquad q = -\frac{w^3}{12\mu}\frac{\mathrm{d}p}{\mathrm{d}x}. \tag{2.5}$$

Boundary conditions on the flow rate q at both ends of the tip cavity can be derived as follows. At the tip of the fracture, the flow rate must necessarily vanish since the width of the channel becomes zero (although the average fluid velocity q/w at the tip does not necessarily vanish)

$$q = 0 \qquad \text{at} \qquad x = 0. \tag{2.6}$$

Note that the non-vanishing of q at the fracture tip would imply, in view of (2.1)–(2.2) and (2.4), an inverse square root singularity in the fluid pressure, which is incompatible with the equations of either linear fracture mechanics or diffusion theory. A condition on q at $x = \lambda$ can be deduced from the assumption of a sharp interface between the fracturing and the pore fluid and the condition of stationarity

$$q = -Vw \qquad \text{at} \qquad x = \lambda. \tag{2.7}$$

It is also worth noting that integration of the continuity equation (2.3) over the tip cavity, taking into account the two boundary conditions (2.6) and (2.7), yields

$$\int_0^\lambda g(x)\,\mathrm{d}x = 0. \tag{2.8}$$

This equation, which could have been deduced directly from the stationarity condition, expresses that the total volume of (incompressible) fluid in the cavity is conserved or, in other words, that the total rate of fluid volume entering/leaving the tip cavity is zero.

2.2.3. *Pore fluid diffusion around the cavity*

Finally, consider the equations describing the evolution of the pore fluid pressure in the porous medium surrounding the tip cavity (Bear 1988). These equations (presented in the fixed coordinate system) are given by the continuity equation for the pore fluid, Darcy law and a constitutive relation

$$\left.\begin{aligned}
\frac{\partial \zeta}{\partial t} &= -\nabla \cdot \boldsymbol{q} + \omega, \\
\boldsymbol{q} &= -(k/\mu)\nabla p, \\
\zeta &= Sp,
\end{aligned}\right\} \tag{2.9}$$

where ζ is the variation of fluid content per unit volume of the porous medium, $\boldsymbol{q}$ is the specific discharge vector, and ω is the source/sink term. Also, k is the intrinsic permeability of the medium and S is the storage coefficient. Equations (2.9) can be combined to yield a diffusion equation for the pore pressure p

$$\frac{\partial p}{\partial t} = c\nabla^2 p + \frac{\mu c}{k}\omega, \tag{2.10}$$

where $c = k/\mu S$ is the diffusivity.

Under the stationarity assumption, (2.10) transforms into a Helmholtz equation in the moving coordinate system (x, y)

$$c\nabla^2 p - V\frac{\partial p}{\partial x} = -\frac{\mu c}{k}\omega. \tag{2.11}$$

The inhomogeneous term ω in (2.11) corresponds to the fluid flux discontinuity across the tip cavity

$$\omega(x, y) = \delta(y)\int_0^\lambda g(u)\,\delta(x - u)\,\mathrm{d}u, \tag{2.12}$$

where δ is the Dirac delta function.

The boundary conditions for (2.11) are given by $p = p_0$ at infinity and by continuity between the pore pressure and the cavity pressure (along $0 \leqslant x \leqslant \lambda$, $y = 0$), as well as continuity of the flux through the common function $g(x)$. The pore pressure field is symmetric with respect to the x-axis, and therefore consistent with the no-flux boundary condition postulated along the fracture outside the lag region ($\partial p/\partial y = 0$ along $y = 0$, with $x < 0$ or $x > \lambda$).

2.2.4. *Behaviour of pressure near the fracture tip*

The nature of the fluid pressure solution near the fracture tip is constrained by a set of equations, obtained by considering linear elastic fracture mechanics, lubrication theory, and diffusion. In particular, the solution must be characterized by a finite rate of the energy expended (i) in the creation of new crack surfaces, (ii) by lubrication flow in the tip cavity, and (iii) by fluid flow in the porous rock.

The weaker constraint arises from linear elastic fracture mechanics, as the fluid pressure consistent with the crack aperture asymptote (2.2) can in principle be singular at the tip, as long as the singularity of $p(x)$ is weaker than $x^{-1/2}$. (The asymptote (2.2) reflects a finite rate of energy dissipated by crack propagation in the rock.) Nevertheless, considerations from lubrication theory further limit the admissible singularity of $p(x)$. In the absence of any exchange of fluid between the tip cavity and the rock, the lubrication equations (2.5), combined with the elastic asymptote (2.2), imply that the fluid pressure has a logarithmic singularity. Any pressure singularity is, however, precluded if the rock is permeable and diffusion of pore fluid is taking place. Indeed, a singularity in the fluid pressure would then cause an infinite rate of energy dissipation by diffusion of fluid in the porous rock.

2.2.5. *Final set of equations*

Formulation of the diffusion problem can be reduced to an integral equation involving only the pressure $p(x)$ in the cavity and the flux discontinuity $g(x)$, by making use of the moving source solution (Carslaw & Jaeger 1959). This solution of (2.11) with $\omega = Q\delta(x)\delta(y)$ (representing a fluid source at the origin of the moving coordinates system and characterized by a constant injection flow rate Q) is given by

$$p = \frac{\mu Q}{2\pi k}\exp\left(\frac{Vx}{2c}\right)\mathrm{K}_0\left[\frac{V}{2c}(x^2 + y^2)^{1/2}\right], \tag{2.13}$$

where K_0 is the modified Bessel function of the second kind (Abramowitz & Stegun 1964). The solution of the diffusion problem with the boundary conditions at infinity and along the tip cavity can then be obtained by integrating the source solution, thus

yielding the integral equation

$$p - p_0 = \frac{\mu}{2\pi k} \int_0^\lambda g(u) \exp\left[\frac{V(x-u)}{2c}\right] \mathrm{K}_0\left[\frac{V|x-u|}{2c}\right] \mathrm{d}u. \tag{2.14}$$

This equation together with the differential equation

$$\frac{\mathrm{d}}{\mathrm{d}x}\left(x^{3/2}\frac{\mathrm{d}p}{\mathrm{d}x}\right) - \frac{3\pi\mu V E'^2}{16 K_{Ic}^2}\frac{1}{x^{1/2}} = \left(\frac{\pi}{2}\right)^{1/2}\frac{3\pi\mu E'^3}{32 K_{Ic}^3}g, \tag{2.15}$$

obtained by combining (2.1)–(2.2), and (2.5) and the boundary conditions

$$x^{3/2}\frac{\mathrm{d}p}{\mathrm{d}x} = 0 \qquad \text{at} \qquad x = 0, \tag{2.16}$$

$$\frac{8\lambda K_{Ic}^2}{3\pi\mu V E'^2}\frac{\mathrm{d}p}{\mathrm{d}x} = 1 \qquad \text{at} \qquad x = \lambda, \tag{2.17}$$

constitute a closed system to be solved for the two functions $p(x)$ and $g(x)$, which are defined for $0 \leqslant x \leqslant \lambda$. The boundary condition at $x = 0$ is automatically satisfied if p is a regular function. Note that (2.14) and (2.15) can be combined into a single integro-differential equation.

2.3. Scaling and dimensionless formulation

As formulated, the tip problem depends on six dimensional parameters which are: the propagation velocity V, the length of the lag zone λ, the ratio of the rock toughness K_{Ic} to the modulus E', the hydraulic diffusivity c, the permeability k and the dynamic viscosity μ (the far-field pore pressure p_0 entering only as a reference value for the fluid pressure). Thus, according to dimensional analysis, the problem depends at most on three dimensionless parameters. However, appropriate scaling of the governing equations shows that the solution depends upon two numbers (and not three), and upon a single one in the asymptotic cases of large or small velocities.

First, it is convenient to introduce two lengthscales ℓ_k and ℓ_d defined as follows

$$\ell_k = \frac{8}{\pi}\left(\frac{K_{Ic}}{E'}\right)^2, \qquad \ell_d = \frac{c}{V}. \tag{2.18}$$

The lengthscale ℓ_k is associated with the fracture mechanics aspect of this problem (the fracture aperture is of order ℓ_k at a distance ℓ_k from the tip), while the lengthscale ℓ_d characterizes the diffusion aspect. (The lengthscale ℓ_d gives a measure of the dimension of the region where the pore pressure is significantly perturbed from the initial value p_0.)

We now introduce several dimensionless quantities: the coordinates (ξ, ζ)

$$\xi = x/\lambda, \quad \zeta = y/\lambda, \tag{2.19}$$

the fracture opening $\Omega(\xi)$, the fluid pressure $\Pi(\xi)$ (or the pore pressure $\Pi(\xi, \zeta)$), the flux discontinuity $\gamma(\xi)$, and the flow rate $\Psi(\xi)$ which are defined as follows

$$\Omega = \frac{w}{w_*}, \quad \Pi = \frac{p - p_0}{p_*}, \quad \Psi = \frac{q}{q_*}, \quad \gamma = \frac{g}{g_*}. \tag{2.20}$$

The characteristic opening in the scaling (2.20) is selected as the maximum tip cavity opening (2.1)–(2.2) taking place at the fluid interface, $w_* = w(\lambda)$,

$$w_* = 4\left(\frac{2}{\pi}\right)^{1/2}\frac{K_{Ic}\lambda^{1/2}}{E'} = 2(\ell_k\lambda)^{1/2}. \tag{2.21}$$

The rest of the characteristic quantities in (2.20) are given by

$$p_* = \frac{3\pi}{8}\left(\frac{E'}{K_{Ic}}\right)^2 \mu V = 12\frac{\mu V \lambda}{w_*^2} = 3\frac{\mu V}{\ell_k}, \tag{2.22}$$

$$q_* = 4\left(\frac{2}{\pi}\right)^{1/2}\frac{K_{Ic}\lambda^{1/2}V}{E'} = w_* V = 2(\ell_k \lambda)^{1/2}V, \tag{2.23}$$

$$g_* = 4\left(\frac{2}{\pi}\right)^{1/2}\frac{K_{Ic}V}{E'\lambda} = \frac{w_* V}{\lambda} = 2\left(\frac{\ell_k}{\lambda}\right)^{1/2}V. \tag{2.24}$$

In scaled form, the governing equations are then written as

$$\Omega = \xi^{1/2}, \tag{2.25}$$

$$\Psi = -\Omega^3\frac{\mathrm{d}\Pi}{\mathrm{d}\xi}, \tag{2.26}$$

$$\frac{\mathrm{d}\Psi}{\mathrm{d}\xi} + \frac{\mathrm{d}\Omega}{\mathrm{d}\xi} = -\gamma, \tag{2.27}$$

$$\Pi = \int_0^1 \Pi_s(\xi - u)\gamma(u)\,\mathrm{d}u, \tag{2.28}$$

and the boundary conditions as $\Psi(0) = 0$ and $\Psi(1) = -1$. The kernel $\Pi_s(\xi)$ in (2.28) is given by

$$\Pi_s(\xi) = \frac{1}{2\pi\varrho}\exp\left(\frac{v\xi}{2}\right)\mathrm{K}_0\left(\frac{v|\xi|}{2}\right), \tag{2.29}$$

where the dimensionless parameters ϱ and v are respectively defined as

$$\varrho = \frac{3\pi^{3/2}}{2^{11/2}}\frac{kE'^3}{\lambda^{1/2}K_{Ic}^3} = 12\frac{k\lambda}{w_*^3} = \frac{3}{2}\frac{k}{\lambda^{1/2}\ell_k^{3/2}}, \tag{2.30}$$

$$v = \frac{V\lambda}{c} = \frac{\lambda}{\ell_d}. \tag{2.31}$$

The solution of the tip problem depends therefore only on two numbers, ϱ and v, which take the simple interpretation of a scaled permeability and a scaled tip velocity, respectively. The number v, which corresponds to the ratio of the cavity size to the diffusive lengthscale, can also be interpreted as a Péclet number.

The solution is characterized by an inverse square root singularity of the flux discontinuity at the tip. It can indeed be deduced from the fluid continuity equation, that the inverse square root singularity introduced by $\mathrm{d}\Omega/\mathrm{d}\xi$ at the tip must necessarily be balanced by γ, since Ψ must behave near $\xi = 0$ as ξ^α with $\alpha > 1/2$ to prevent any singularity in Π, according to (2.26); hence, $\gamma \sim -\xi^{-1/2}$ as $\xi \to 0$.

It is also useful to introduce the integral $\Upsilon(\xi)$ of the flux discontinuity γ across the crack tip

$$\Upsilon = \int_0^\xi \gamma(u)\,\mathrm{d}u. \tag{2.32}$$

The function $\Upsilon(\xi)$ gives the outflow rate of fluid volume exchanged between the cavity and the porous medium from the tip to a point ξ. Note that $\Upsilon(\xi) \leqslant 0$ with $\Upsilon(0) = \Upsilon(1) = 0$ and that its minimum value $\Upsilon_{min} \geqslant -1$. Indeed, integration of the continuity equation (2.27) yields

$$\Upsilon = -\Omega - \Psi. \tag{2.33}$$

Finally, the system of equations can be reduced to a single integro-differential equation in Π, accounting for both the diffusion in the porous medium and the fluid flow in the cavity; this equation is obtained by substituting into (2.28) the expression for the source density γ given by the lubrication equation

$$\frac{d}{d\xi}\left(\xi^{3/2}\frac{d\Pi}{d\xi}\right) - \frac{1}{2\xi^{1/2}} = \gamma, \tag{2.34}$$

(which is derived from the continuity equation (2.27) and Poiseuille law (2.26)). The resulting equation

$$\int_0^1 \Pi_s(\xi - u; \varrho, v)\left[\frac{d}{du}\left(u^{3/2}\frac{d\Pi}{du}\right) - \frac{1}{2u^{1/2}}\right] du = \Pi(\xi), \tag{2.35}$$

together with the boundary condition (2.17)

$$\frac{d\Pi}{d\xi} = 1 \qquad \text{at} \qquad \xi = 1, \tag{2.36}$$

completely define the non-singular fluid pressure in the fracture tip cavity. (As noted earlier, the non-singularity of the pressure at the tip automatically satisfies the zero flow rate condition (2.16) at the tip.)

Once the fluid pressure in the cavity $\Pi(\xi)$ has been solved, the flow rate Ψ and flux discontinuity γ are determined from (2.26) and (2.27). With γ known, the pore pressure field $\Pi(\xi, \zeta)$ in the porous medium can then be computed from the convolution integral

$$\Pi = \int_0^1 \Pi_g(\xi - u, \zeta; \varrho, v)\gamma(u)\,du, \tag{2.37}$$

where

$$\Pi_g(\xi, \zeta; \varrho, v) = \frac{1}{2\pi\varrho}\exp\left(\tfrac{1}{2}v\xi\right)\mathrm{K}_0\left[\tfrac{1}{2}v(\xi^2 + \zeta^2)^{1/2}\right]. \tag{2.38}$$

Since there is no net fluid exchanged between the tip cavity and the porous medium, the far-field pore pressure perturbation corresponds to an effective dipole located at the tip and oriented along the ξ-axis with the strength S of the dipole given by

$$S = \int_0^1 \Upsilon(\xi)\,d\xi. \tag{2.39}$$

Note that since the net fluid exchange is zero, dipole strength S is equivalent to the moment of the source density γ along the cavity, i.e. $S = \int_0^1 (\xi - u)\gamma(u)\,du$. With the help of (2.33), (2.25) and (2.26), the dipole strength S can also be expressed in terms of the dimensionless pressure in the cavity

$$S = -\tfrac{2}{3} + \Pi(1) - \tfrac{3}{2}\int_0^1 \xi^{1/2}\Pi(\xi)\,d\xi. \tag{2.40}$$

2.4. *Range of parameters*

It is of interest to estimate the length scales ℓ_k, ℓ_d, w_* and λ, as well as the possible range of variation of the two governing dimensionless parameters ϱ and v. Typically, the rock toughness $K_{Ic} = O(1)$ MPa m$^{1/2}$ and the elastic modulus $E' = O(10^4)$ MPa. In contrast, the rock permeability k varies over many orders of magnitude, from 10^{-21} m^2 for shales to 10^{-12} m^2 for permeable sandstones; the corresponding diffusivity

		Dykes	HF
E'	(GPa)	30	30
K_{Ic}	(MPa m$^{1/2}$)	1	1
μ_f	(Pa s)	10	0.1
σ_0	(MPa)	100	10
V	(m s^{-1})	10	1
ℓ_k	(m)	3×10^{-9}	3×10^{-9}
λ	(m)	1	0.1
w_*	(m)	10^{-4}	3×10^{-5}
k	(m^2)	10^{-18}	$10^{-21} - 10^{-12}$
c	(m^2 s^{-1})	10^{-6}	$10^{-7} - 1$
ℓ_d	(m)	10^{-7}	$10^{-7} - 1$
ϱ		10^{-5}	$10^{-7} - 10^2$
v		10^7	$10^6 - 10^{-1}$
η		$10^{-1.5}$	$10^{-4} - 10^{1.5}$

TABLE 1. Estimates of the lag λ, (2.41), length scales ℓ_k, ℓ_d, (2.18), and w_*, (2.21); dimensionless permeability ϱ, (2.30), dimensionless velocity v, (2.31), and dimensionless permeability in the large velocity case, η, (5.3), corresponding to plausible values/ranges of rock and fracturing fluid material constants, and confining stress levels and propagation velocities of dykes and hydraulic fractures (HF).

c varying from 10^{-7} m^2 s^{-1} to 1 m^2 s^{-1}. In the case of dyke propagation, typical values of the permeability and diffusivity of the host granitic or basaltic rock are 10^{-18} m^2 and 10^{-6} m^2 s^{-1}, respectively.

Apart from the above material parameters, the length of the tip cavity λ and the fracture propagation velocity V are both functions of the solution for the finite crack (i.e. the outer solution). In impermeable rocks where the tip cavity is at zero pressure, λ depends on the outer solution only via the tip velocity V provided that λ is small compared to the crack dimension. Under these conditions, the solution of a semi-infinite fluid-driven fracture in an impermeable rock yields the following estimate for the maximum lag (Garagash & Detournay 2000)

$$\lambda \simeq \frac{4\mu_f E'^2 V}{\sigma_0^3}, \tag{2.41}$$

where μ_f is the fracturing fluid viscosity and σ_0 is the *in situ* stress perpendicular to the fracture plane. Estimates for the fracturing fluid viscosity specific to dykes and hydraulic fractures were cited in §1. The confining stress is of order of the lithostatic pressure, and thus dependent on the depth; typically, $\sigma_0 = 10 \sim 100$ MPa. Although the tip velocity V can readily be computed for simple fracture geometries given the boundary conditions, it is sufficient here to state that generally $V = 0.1 \sim 10$ m s^{-1}.

Table 1 summarizes relevant values of the problem parameters for dykes and for hydraulic fractures, as well as appropriate ranges for the dimensionless permeability ϱ and propagation velocity v. This table indicates that the dyke problem is characterized by a small ϱ (attributable to the large magma viscosity μ_f and the small permeability k of the host rock) and by a large v (attributable to the small diffusivity of the host rock). On the other hand, ϱ and v for hydraulic fractures can vary over many orders of magnitude, owing mainly to the wide range of permeability of the reservoir rock. For example, the rocks at the lower end of the permeability interval correspond to the minimum ϱ and maximum v of the range, whereas rocks at the upper end of the

permeability interval correspond to the maximum ϱ and minimum v of the range, see table 1.

Table 1 and the above observations suggest that the large v asymptotic solution is relevant for the propagation of dykes. The solution in the complete range (small to large) of v and ϱ is required to represent hydraulic fractures in various rocks.

3. Asymptotic limits for small and large permeability ϱ

It is of interest to identify the two limits of zero and infinite permeability ϱ. Consider first the limit $\varrho \to 0$. Multiplying (2.28) by ϱ and taking the limit of the resulting expression for $\varrho \to 0$ shows that the source density is everywhere zero in the tip cavity, $\gamma \equiv 0$. Hence, the limit $\varrho = 0$ corresponds to a situation where there is no fluid exchanged between the medium and the cavity. This conclusion could indeed have been deduced by noting that the lower limit of ϱ can be reached for a material with zero permeability, $k = 0$. (Although the diffusivity c also goes to zero in the limit of $k = 0$, c can always be expressed as $c = k/\mu S$, where S is a fluid storage coefficient; hence ϱ goes to zero as $k^{1/2}$). Hence, this limiting case corresponds to a fracture driven in an impermeable rock by two fluids of different viscosities (μ_f and μ), with one fluid (μ) confined to a region with extent λ in the fracture tip by the other fluid (μ_f). The pressure in the tip cavity follows from (2.25)–(2.27) with $\gamma \equiv 0$

$$\Pi(\xi) = 2(1 - \ln 2) + \ln \xi. \tag{3.1}$$

Hence, the interface pressure $\Pi(1)$ tends towards a finite value in the limit of $\varrho = 0$

$$\lim_{\varrho \to 0} \Pi(1) = 2(1 - \ln 2). \tag{3.2}$$

The limit $\varrho = 0$ yields, therefore, a negative logarithmic singularity in the fluid pressure at the fracture tip. The fluid would then necessarily cavitate in the vicinity of the tip, and the solution $\varrho = 0$ is thus clearly inconsistent with the assumption of an incompressible fluid completely occupying the tip cavity. A consistent solution for the limiting case of an impermeable rock requires consideration of a lag region between the fracturing fluid and the tip of the fracture, which is devoid of fluid. (Although the tip cavity would be filled by vapours from the fracturing fluid, the vapour pressure could conveniently be considered as zero in comparison with the magnitude of the *in situ* stress σ_0.) Such a solution that takes into account the existence of a lag of *a priori* unknown length can indeed be constructed (Garagash & Detournay 2000).

It is also worth mentioning that a small perturbation of the $\varrho = 0$ solution is singular (Kevorkian & Cole 1996), since the source density is infinite at the fracture tip ($\gamma \sim -\xi^{-1/2}$) for any non-zero ϱ, while it is identically zero for $\varrho = 0$. Thus, the structure of the solution in the case of a small but non-zero permeability ϱ is given by the solution $\gamma = 0$ away from the fracture tip, and by a boundary-layer solution incorporating the singular γ near the fracture tip. As shown later, the source density has a positive singularity at the interface between the fracturing and cavity fluid, as well. Thus, the solution for $\varrho \ll 1$ is characterized by boundary layers at both $\xi = 0$ and $\xi = 1$, which can be viewed as point-sink and point-source on the lengthscale of the tip cavity, respectively.

Consider next the case where ϱ tends to ∞. Here, the net pressure is identically zero, $\Pi \equiv 0$ according to (2.28)–(2.29). For this limit, the fluid continuity equation reduces to

$$\Omega(\xi) + \Upsilon(\xi) = 0 \tag{3.3}$$

everywhere in the cavity except at $\xi = 1$ (since $\Omega(1) = 1$ and $\Upsilon(1) = 0$). The degenerated continuity equation (3.3) reveals a situation where the creation of new space caused by propagation of the crack is instantaneously filled by fluid flowing from the formation. In other words, the fluid infiltration velocity consistent with a uniform pressure in the tip region exactly balances the rate of change of the crack opening. A Dirac singularity for the flux discontinuity γ must nonetheless necessarily take place at $\xi = 1$ in order to enforce the constant fluid volume in the crack tip cavity (hence, the singularity in the pressure at $\xi = 1$).

4. Asymptotic solution for small velocity v

4.1. *Singular integral equation*

We first consider the case of small propagation velocity, $v \ll 1$. According to the definition (2.31) of v, this asymptotic case corresponds to situations where the diffusion length c/V is large compared to the cavity length λ. The integro-differential equation (2.35) can be simplified for small v by expanding the kernel $\Pi_s(\xi - u; \varrho, v)$ in v and retaining only the first term of the expansion

$$\Pi_s(\xi; \varrho, v) \approx -\frac{1}{2\pi\varrho} \left(\ln\frac{v}{2} + \ln|\xi| \right) \quad \text{for } v \ll 1. \tag{4.1}$$

Since $\Upsilon(1) = 0$, (2.28) becomes

$$\Pi(\xi) = -\frac{1}{2\pi\varrho} \int_0^1 \ln|\xi - u|\gamma(u)\,\mathrm{d}u. \tag{4.2}$$

By integrating by parts the integral in (4.2), using the integral $\Upsilon(\xi)$ of the flux discontinuity γ across the tip cavity given by (2.32), we obtain a singular integro-differential equation with a Cauchy kernel

$$\Pi(\xi) = \frac{1}{2\pi\varrho} \int_0^1 \frac{\Upsilon(u)}{u - \xi}\,\mathrm{d}u \tag{4.3}$$

with boundary conditions on $\Upsilon(\xi)$ given by

$$\Upsilon(0) = \Upsilon(1) = 0. \tag{4.4}$$

In the limiting case of small velocity, the solution thus depends on the dimensionless permeability ϱ only.

Following the classical theory of the Cauchy singular integral equation (Muskhelishvili 1977), (4.3) can be inverted to yield (see Appendix A)

$$\Upsilon(\xi) = -\frac{2\varrho}{\pi} \xi^{1/2}(1 - \xi)^{1/2} \int_0^1 \frac{\Pi(u)}{u^{1/2}(1 - u)^{1/2}} \frac{\mathrm{d}u}{u - \xi}, \tag{4.5}$$

which takes into account (4.4). It can be shown that if the net pressure $\Pi(\xi)$ is finite along the cavity (including the ends), then the integral in (4.5) is a regular function bounded at the cavity ends. Consequently, the source density $\gamma = \mathrm{d}\Upsilon/\mathrm{d}\xi$ has an inverse square root singularity both at the fracture tip $\xi = 0$ and at the fluid interface $\xi = 1$. The source density singularity at the fracture tip has been discussed earlier for an arbitrary v, while the singularity at the fluid interface, which was shown to exist for small v, is expected to hold in the case of finite velocities v as well.

Let us denote the pressure gradient as $\Xi(\xi) = \mathrm{d}\Pi/\mathrm{d}\xi$. By integrating by parts the Cauchy integral in (4.5) and using

$$\Upsilon(\xi) = \xi^{3/2}\Xi(\xi) - \xi^{1/2}, \tag{4.6}$$

obtained by integration of (2.34), a Fredholm integral equation in terms of the pressure gradient $\Xi(\xi)$ can then be deduced

$$\xi^{3/2}\,\Xi(\xi) + \frac{2\varrho}{\pi}\int_0^1 K(\xi, u)\,\Xi(u)\,\mathrm{d}u = \xi^{1/2}. \tag{4.7}$$

In the above, $K(\xi, u)$ denotes the weakly singular kernel

$$K(\xi, u) = \ln\left|\frac{u^{1/2} + \xi^{1/2}}{u^{1/2} - \xi^{1/2}}\,\frac{1 + (1-u)^{1/2}(1-\xi)^{1/2} - u^{1/2}\xi^{1/2}}{1 + (1-u)^{1/2}(1-\xi)^{1/2} + u^{1/2}\xi^{1/2}}\right|. \tag{4.8}$$

4.2. Reduction to a system of linear equations

Application of the coordinate transformations

$$u = \cos^2\theta, \quad \xi = \cos^2\varphi, \tag{4.9}$$

to (4.7) yields

$$\cos^3\varphi\,\bar\Xi(\varphi) + \frac{2\varrho}{\pi}\int_0^{\pi/2}\sin 2\theta\,\bar K(\varphi, \theta)\,\bar\Xi(\theta)\,\mathrm{d}\theta = \cos\varphi \tag{4.10}$$

with the notational convention that $\bar\Xi(\varphi) = \Xi(\cos^2\varphi)$. The kernel $\bar K(\varphi, \theta) = K(\cos^2\varphi, \cos^2\theta)$ is given by the double sine series, see Appendix A

$$\bar K(\varphi, \theta) = \sum_{n=1}^{\infty}\frac{2}{n}\sin 2n\varphi \sin 2n\theta. \tag{4.11}$$

The sine series of $\bar\Upsilon(\varphi) = \cos^3\varphi\,\bar\Xi(\varphi) - \cos\varphi$ is obtained by substituting the expansion (4.11) for $\bar K(\varphi, \theta)$ in (4.10) and integrating term by term. Using this expansion for $\bar\Upsilon(\varphi)$ in (4.3), transformed according to (4.9), yields the series expansion $\bar\Pi(\varphi)$. These two expansions are

$$\bar\Upsilon(\varphi) = \sum_{n=1}^{\infty}\lambda_n \sin 2n\varphi, \tag{4.12}$$

$$\bar\Pi(\varphi) = -\frac{1}{2\varrho}\sum_{n=1}^{\infty}\lambda_n \cos 2n\varphi, \tag{4.13}$$

with the still unknown coefficients λ_n given by

$$\lambda_n = -\frac{4\varrho}{n\pi}\int_0^{\pi/2}\sin 2\theta \sin 2n\theta\,\bar\Xi(\theta)\,\mathrm{d}\theta. \tag{4.14}$$

The expressions for the overall characteristics of the solution, taken as the net pressure at the fracture tip and at the fluid interface and the effective dipole strength S, can be easily deduced from (4.12)–(4.13) as

$$\Pi(0) = -\frac{1}{2\varrho}\sum_{n=1}^{\infty}(-1)^n\lambda_n, \quad \Pi(1) = -\frac{1}{2\varrho}\sum_{n=1}^{\infty}\lambda_n, \quad S = \tfrac{1}{4}\pi\lambda_1. \tag{4.15}$$

The expression for the source density $\bar{\gamma}(\varphi)$ is derived from (4.12) as follows

$$\bar{\gamma}(\varphi) = \frac{\mathrm{d}\bar{\Upsilon}(\varphi)}{\mathrm{d}\varphi}\frac{\mathrm{d}\varphi}{\mathrm{d}\xi} = -\frac{1}{\sin 2\varphi}\sum_{n=1}^{\infty} 2n\lambda_n \cos 2n\varphi. \tag{4.16}$$

The functions $\Upsilon(\xi)$, $\Pi(\xi)$ and $\gamma(\xi)$ are finally deduced from $\bar{\Upsilon}(\varphi)$, $\bar{\Pi}(\varphi)$ and $\bar{\gamma}(\varphi)$, through the substitution $\varphi = \arccos(\xi^{1/2})$. It is seen from (4.16) that the source density $\gamma(\xi)$ has an inverse square root singularity at both ends of the tip cavity

$$\gamma \simeq -\frac{1}{2\xi^{1/2}} \quad \text{as} \quad \xi \to 0, \tag{4.17}$$

$$\gamma \simeq -\frac{A}{2\left(1-\xi\right)^{1/2}} \quad \text{as} \quad \xi \to 1 \quad \text{with} \quad A = \sum_{n=1}^{\infty} 2n\lambda_n. \tag{4.18}$$

The infinite system of linear algebraic equations in the unknown coefficients λ_n is formulated by substituting the series expression for $\bar{\Xi}(\varphi)$, derived from (4.13) into the integral of (4.14). Hence,

$$\sum_{m=1}^{\infty} \left[\phi_{nm} + \frac{n\pi}{4\varrho}\delta_{nm}\right]\lambda_m = -\psi_n, \quad n = 1,\ldots,\infty, \tag{4.19}$$

where δ_{nm} is the Kronecker delta, and the coefficients ϕ_{nm} and ψ_n are given by

$$\phi_{nm} = \int_0^{\pi/2} \frac{\sin 2\theta}{\cos^3\theta}\sin 2n\theta \sin 2m\theta\, \mathrm{d}\theta, \tag{4.20}$$

$$\psi_n = \int_0^{\pi/2} \frac{\sin 2\theta}{\cos^2\theta}\sin 2n\theta\, \mathrm{d}\theta. \tag{4.21}$$

The integrals in (4.20) and (4.21) are known explicitly, hence

$$\phi_{nm} = \sum_{k=0}^{m+n-1}\left(\frac{k+1/4}{m+n}-\frac{1}{2}\right)^{-1} - \sum_{k=0}^{|m-n|-1}\left(\frac{k+1/4}{|m-n|}-\frac{1}{2}\right)^{-1}, \tag{4.22}$$

$$\psi_n = (-1)^{n+1}\pi. \tag{4.23}$$

An approximate solution $\lambda_1^{(N)},\ldots,\lambda_N^{(N)}$ is sought here by truncating the system (4.19) to N equations into N unknowns

$$\sum_{m=1}^{N}\left[\phi_{nm} + \frac{n\pi}{4\varrho}\delta_{nm}\right]\lambda_m^{(N)} = -\psi_n, \quad n = 1,\ldots,N. \tag{4.24}$$

Note that this solution satisfies the conditions that for any $\epsilon > 0$, there exists an $N(\varrho, \epsilon)$ such that $|\lambda_N^{(N)}| < \epsilon$, $|\lambda_i^{(N)} - \lambda_i^{(M)}| < \epsilon$, and $\sum_{i=N}^{M}|\lambda_i^{(M)}| < \epsilon$ for any $M > N$ and any i in the interval $[1,\ldots,N]$. Therefore, the truncated system of $N(\varrho, \epsilon)$ equations (4.24) provides a solution of order ϵ of the full system (4.19); i.e. $\lambda_i = \lambda_i^{(N)}$ for $i = 1,\ldots,N$ and $\lambda_i = 0$ for $i > N$.

5. Asymptotic solution for large velocity v

5.1. *Closed-form solution*

Next, we consider the limiting case of large fracture propagation velocity, $v \gg 1$, corresponding to cases where the diffusion length c/V is small compared to the cavity

length λ. The particular integro-differential equation in Π for large v can be derived from the general integral equation (2.35), see Appendix B for details. Alternatively, this equation can be derived from *ad hoc* considerations of so-called linear flow. Using the asymptotic formula of the Bessel function $K_0(\zeta)$ for large ζ, it can be shown that the convolution integral in (2.28) can be written as

$$\frac{1}{2\pi\varrho} \int_0^1 \exp\left(\frac{v(\xi - u)}{2}\right) K_0\left(\frac{v|\xi - u|}{2}\right) \gamma(u)\, \mathrm{d}u \approx \frac{1}{2\varrho\sqrt{\pi v}} \int_0^\xi \frac{\gamma(u)}{(\xi - u)^{1/2}}\, \mathrm{d}u \quad \text{for } v \gg 1.$$
(5.1)

The integral equation (2.35) can thus be reduced to

$$\frac{2}{\pi} \int_0^\xi \frac{\mathrm{d}}{\mathrm{d}u}\left(u^{3/2}\frac{\mathrm{d}\Pi}{\mathrm{d}u}\right) \frac{1}{(\xi - u)^{1/2}}\, \mathrm{d}u = 1 + \eta\Pi(\xi),$$
(5.2)

where

$$\eta = 4\varrho\left(\frac{v}{\pi}\right)^{1/2} = \frac{6k}{\left(\pi\ell_d\ell_k^3\right)^{1/2}}.$$
(5.3)

The number η is thus the only parameter controlling the solution when v is large. The merging of the two numbers ϱ and v into the single parameter η, according to (5.3), is to be expected because the solution should not depend on the cavity length λ in the limit of linear flow. The range of variation of η is $[0, \infty[$.

Consider now a solution of the integral equation (5.2) in the form

$$\Pi(\xi) = C + \frac{1}{\alpha}\xi^\alpha, \quad \alpha > -\tfrac{1}{2},$$
(5.4)

where C and α are unknown constants. The form (5.4) already satisfies the boundary condition (2.36). Substitution of (5.4) into (5.2) and integration yields

$$\frac{(1 + 2\alpha)\Gamma\left(\tfrac{1}{2} + \alpha\right)}{\pi^{1/2}\Gamma(1 + \alpha)}\xi^\alpha = 1 + \eta C + \frac{\eta}{\alpha}\xi^\alpha,$$
(5.5)

where Γ is the Euler gamma function. Matching of terms in (5.5) yields the explicit value for the unknown constant C and an algebraic equation for the power exponent α

$$C = -\frac{1}{\eta},$$
(5.6)

$$\eta = f(\alpha),$$
(5.7)

where

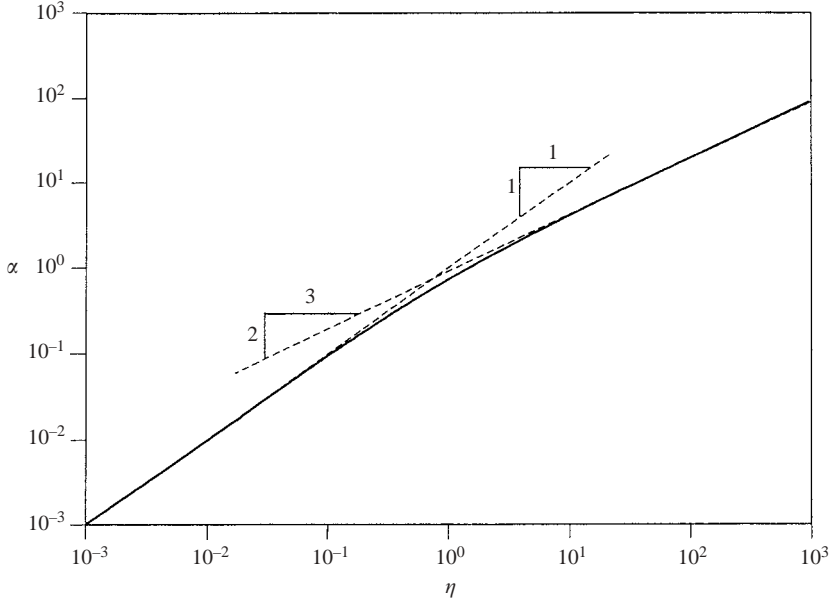$$f(\alpha) = \frac{\alpha(1 + 2\alpha)\Gamma\left(\tfrac{1}{2} + \alpha\right)}{\pi^{1/2}\Gamma(1 + \alpha)}.$$
(5.8)

It can readily be shown that $f(\alpha) \sim \alpha$ for $\alpha \ll 1$ and $f(\alpha) \sim 2\pi^{-1/2}\alpha^{3/2}$ for $\alpha \gg 1$; hence,

$$\alpha \sim \eta \qquad \text{for} \qquad \eta \ll 1,$$
(5.9)

$$\alpha \sim \frac{\pi^{1/3}}{2^{2/3}}\eta^{2/3} \qquad \text{for} \qquad \eta \gg 1.$$
(5.10)

The solution $\alpha(\eta)$ of (5.7) is plotted in figure 2, together with the two asymptotes (5.9) and (5.10).

FIGURE 2. Pressure exponent α versus number η in log–log scale.

Finally, the solutions for the fluid pressure Π, flow rate Ψ, source density γ, and integral of the source density Υ take the form

$$\Pi = \frac{1}{\eta}\left(\frac{\eta}{\alpha}\xi^{\alpha} - 1\right), \tag{5.11}$$

$$\Psi = -\xi^{\alpha+1/2}, \tag{5.12}$$

$$\gamma = \frac{1}{2\xi^{1/2}}[(1+2\alpha)\xi^{\alpha} - 1], \tag{5.13}$$

$$\Upsilon = \xi^{\alpha+1/2} - \xi^{1/2}, \tag{5.14}$$

where $\alpha = \alpha(\eta)$ is the solution of (5.7).

Since $\alpha > 0$ for $\eta > 0$, the fluid pressure in the cavity is always a regular function bounded everywhere along the cavity. The pressure monotonically increases from the tip ($\xi = 0$) to the interface between the cavity and the rest of the crack ($\xi = 1$) with the minimum of the pressure reached at the tip $\Pi(0) = -1/\eta$ and the maximum at the interface between the two fluids $\Pi(1) = 1/\alpha - 1/\eta$.

Some other information about the flow of pore fluid in and out of the cavity is given by the minimum Υ_{min} (corresponding to $\gamma = 0$) which takes place at $\xi = \xi_*$ and is given by

$$\xi_* = \frac{1}{(1+2\alpha)^{1/\alpha}}, \tag{5.15}$$

and thus

$$\Upsilon_{min} = -2\alpha\left(\frac{1}{1+2\alpha}\right)^{1+1/2\alpha}. \tag{5.16}$$

So indeed, Υ_{min} decreases from 0 to -1 as α varies from 0 to ∞ (note that ξ_* varies from e^{-2} to 1). To characterize this dipole we compute its strength S according

to (2.39),

$$S = -\frac{4\alpha}{3(3 + 2\alpha)}. \tag{5.17}$$

5.2. *Asymptotic limits for small and large η*

First, it is of interest to introduce another characteristic pressure $\overline{p}_*$ defined as

$$\overline{p}_* = \frac{p_*}{\eta} = (\pi\ell_d\ell_k)^{1/2}\frac{\mu V}{2k}. \tag{5.18}$$

and the alternative pressure scaling $\overline{\Pi}$

$$\overline{\Pi} = \frac{p - p_0}{\overline{p}_*}. \tag{5.19}$$

The solution for the fluid pressure in the cavity can thus be rewritten as

$$\overline{\Pi} = \frac{\eta}{\alpha}\xi^a - 1. \tag{5.20}$$

According to (5.11), the dimensionless pressure at the fracture tip is $\overline{\Pi}(0) = -1$; translated into absolute terms, this means that the pressure at the tip, $p_{tip} = p_0 - \overline{p}_*$. Obviously, the model applies as long as $p_{tip} > 0$ (pragmatically), i.e. $\overline{p}_* < p_0$, as otherwise cavitation would take place.

It can be readily established from the relation of the parameter η to the dimensionless permeability ϱ, (5.3), and the form of the large v solution, that asymptotic limits of the latter for small and large η are identical to the small and large ϱ limiting solutions discussed above. However, consideration of the solution in the alternative pressure scaling provides additional information about the solution structure in the limit $\eta \to \infty$. Indeed, in the original pressure scaling, Π vanishes everywhere in the tip cavity as $\eta \to \infty$. However, the rescaled fluid cavity pressure $\overline{\Pi}$ (ξ) tends towards the constant tip pressure $\overline{\Pi} = -1$ in the limit $\eta \to \infty$, except at the fluid interface $\xi = 1$ where the pressure becomes singular ($\overline{\Pi}(1) \to \infty$ as $\eta^{1/3}$). However, it does not appear that this limit can be realistically approached, in view of the admissible range of variations of the basic parameters, and under the condition that v is large (see also table 1).

6. General solution for arbitrary velocity v

To find the solution for an arbitrary v, we express the equations in terms of the source density γ. Consider (4.6) which is here written as

$$\xi^{3/2}\frac{\mathrm{d}\Pi}{\mathrm{d}\xi} = \xi^{1/2} + \int_0^\xi \gamma(u)\,\mathrm{d}u. \tag{6.1}$$

As discussed previously, $\gamma(\xi)$ has an inverse square root singularity at the tip (which can be confirmed from an examination of (6.1)); hence, we represent $\gamma(\xi)$ as

$$\gamma = -\tfrac{1}{2}\xi^{-1/2} + \gamma_r, \quad \gamma_r = O(\xi^{-1/2+\alpha}), \quad \alpha > 0, \tag{6.2}$$

where $\gamma_r(\xi)$ is a source density 'regularized' at the fracture tip. (According to the preceding discussion of the small v case, $\gamma_r(\xi)$ may still have a singularity at the fluid interface $\xi = 1$). Substituting (6.2) into (6.1) and integrating with respect to ξ, we arrive at the expression of the pressure inside the cavity Π in terms of $\gamma_r(\xi)$

$$\Pi = \Pi(0) - \frac{2}{\xi^{1/2}}\int_0^\xi \gamma_r(u)\,\mathrm{d}u + 2\int_0^\xi \frac{\gamma_r(u)}{u^{1/2}}\,\mathrm{d}u, \tag{6.3}$$
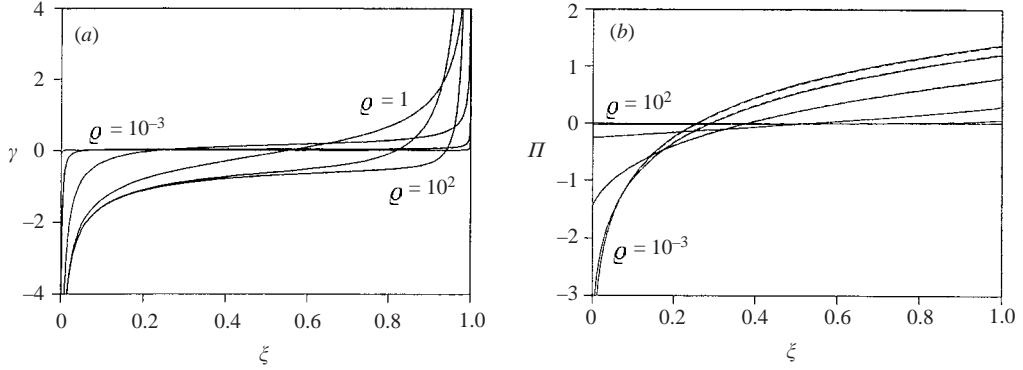
FIGURE 3. Variation of (*a*) the source density γ and (*b*) the fluid pressure Π along the cavity for $v = 10^{-2}$ and various $\varrho = 10^{-3}, \cdots, 10^2$. The numerical solution (based on the algorithm for arbitrary v) and small v asymptotic solution are shown by solid and dashed lines, respectively. (Note that for a given choice of $v = 10^{-2}$ the two solutions are practically identical).

where $\Pi(0)$ is the value of the pressure at the tip. An integral equation in γ_r, involving also the unknown tip pressure $\Pi(0)$ can then be deduced from (2.28) and (6.3),

$$\Pi_t(\xi) + \int_0^1 \Pi_s(\xi - u, 0)\gamma_r(u)\, du = \Pi(0) - 2\xi^{-1/2} \int_0^\xi \gamma_r(u)\, du + 2 \int_0^\xi u^{-1/2}\gamma_r(u)\, du,$$

(6.4)

where $\Pi_t(\xi)$ is the part of the integral in (2.28) corresponding to the singularity of γ at the tip

$$\Pi_t(\xi) = -\tfrac{1}{2} \int_0^1 \Pi_s(\xi - u, 0)u^{-1/2}\, du.$$

(6.5)

Equation (6.4) is complemented by an integral condition which results from (2.8)

$$\int_0^1 \gamma_r(\xi)\, d\xi = 1.$$

(6.6)

Summarizing, the integral equation (6.4) with the integral constraint (6.6) completely define the 'regularized' source density $\gamma_r(\xi)$ and the tip pressure $\Pi(0)$ as a function of the two dimensionless numbers v and ϱ. (Equivalently, the dimensionless cavity fluid pressure $\Pi(\xi)$ can be solved from the integral equation (2.35) and the boundary condition (2.36)). This problem is solved numerically, see Appendix C for details of the method used. Once this solution is found, $\gamma(\xi)$ and $\Pi(\xi)$ are computed using (6.2) and (6.3), respectively.

7. Numerical results
7.1. *Arbitrary velocity solution and asymptotic solutions*
First, we discuss the numerical solution for the source density γ and net-pressure Π along the cavity obtained with the numerical algorithm for arbitrary velocity v and compare this numerical solution to the small and large v asymptotic solutions. Figures 3, 4 and 5 show the distribution of the source density γ and the pressure Π for $v = 10^{-2}$, 10^2 and 10^4, and various values of ϱ ranging from 10^{-3} to 10^2. The numerical solution computed with the algorithm for arbitrary v is shown by solid
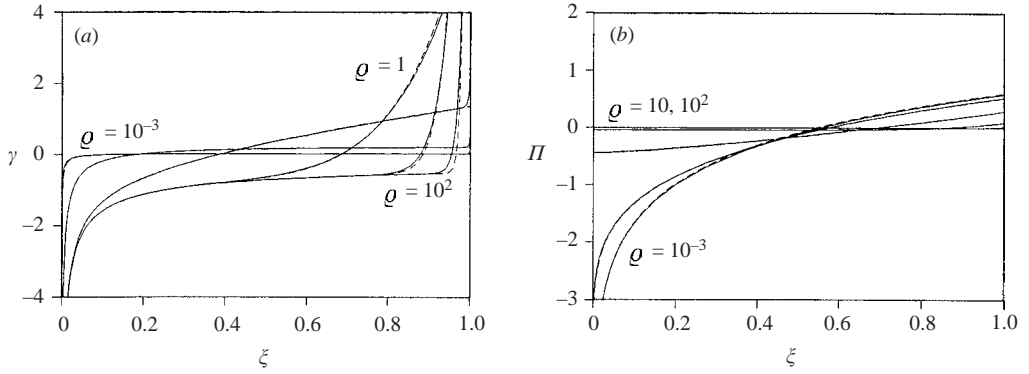
FIGURE 4. Variation of (*a*) the source density γ and (*b*) the fluid pressure Π along the cavity for $v = 10^2$ and various $\varrho = 10^{-3}, \cdots, 10^2$. The numerical solution for arbitrary v and the large velocity asymptotic solution are shown by solid and dashed lines, respectively.
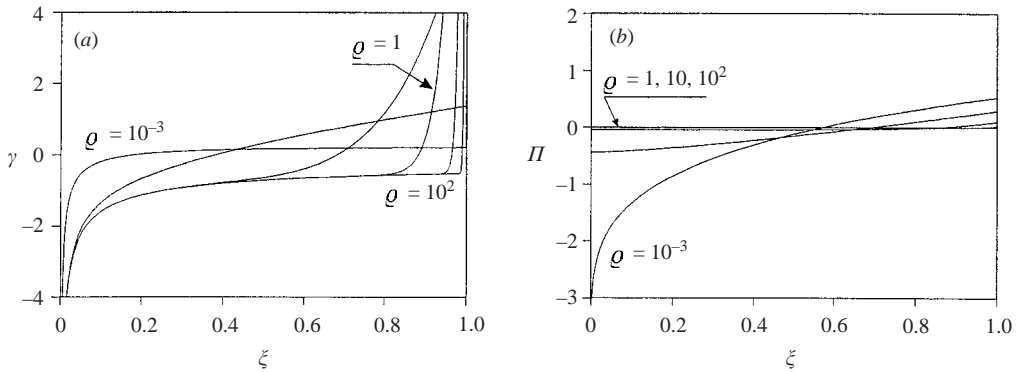

FIGURE 5. Variation of (*a*) the source density γ and (*b*) the fluid pressure Π along the cavity for $v = 10^4$ and various $\varrho = 10^{-3}, \cdots, 10^2$. The numerical solution for arbitrary v is identical to the large v asymptotic solution.

lines, whereas the asymptotic solutions are shown in dashed lines in these figures. (Calculations with the general algorithm were performed with $N = 300$ collocation points, while the computations with the small v algorithm were carried out with $N = 400$; the large v asymptote is computed for the set of values of the parameter $\eta = 4\varrho/(\pi v)^{1/2}$ corresponding to v equal either to 10^2 or to 10^4, and the given set of ϱ values). Figure 3 shows hardly any differences between the small v asymptotic solution (dashed lines) and the solution for $v = 10^{-2}$ (solid lines). Similarly, the large v asymptotic solution is virtually identical to the numerical solution $v = 10^4$, as can be seen in figure 5. The large v asymptotic solution is a very good approximation for v as low as 10^2, except for the source density near the fluid interface $\xi = 1$ (see figure 4). Although the numerical solution suggests a singular behaviour for γ at $\xi = 1$, the large v asymptotic solution indicates that γ is finite at the interface between the two fluids. Thus, we can conclude that the tip cavity solution is practically given by its small v asymptote for $v \leqslant 10^{-2}$ and by its large v asymptotic solution for $v \geqslant 10^2$.

Figures 3–5 show qualitatively very similar distributions of the source density and net-pressure in the tip cavity and their dependence on the permeability ϱ. The

numerical solution for the source density confirms that the source density has a negative inverse square root singularity at the fracture tip. It also predicts a positive singularity for the source density at the fluid interface $\xi = 1$, the physical nature of which is not yet well understood. The source density is seen to increase monotonically from negative infinity at the fracture tip to a positive infinity at the fluid interface. The source density thus vanishes at a point along the cavity; this point separates the cavity into two adjacent regions: one where the pore fluid is sucked into the cavity, the other one where the fluid is leaking off the cavity. The position of the transition point is moving from the tip to the interface as the permeability ϱ increases from zero to infinity. For small ϱ, suction of the pore fluid occurs only in the very close vicinity of the tip while leak-off takes place over most of the length of the cavity; for large ϱ, pore fluid is sucked into the cavity along most of the cavity length and is expelled from the cavity only in the small region adjacent to the fluid interface between the cavity and the rest of the crack. For small ϱ, the source density distribution is very similar to a sink/source pair, with the sink at the tip and the source at the interface; in other words, the source density is almost zero over the most of the tip cavity and singular with opposite sign at the two ends of the cavity. Comparison of figures 3(a)–5(a) indicates that the zone of pore fluid suction adjacent to the fracture tip expands with increasing velocity v for a fixed permeability ϱ.

The dimensionless fluid pressure Π is negative at the tip and positive at the fluid interface, see figures 3(b)–5(b). (According to the scaling, it corresponds to a fluid pressure p smaller (greater) then the far-field pore pressure p_0 at the tip of the fracture $\xi = 0$ (at the fluid interface $\xi = 1$)). The pressure Π increases monotonically from a negative tip value to a positive fluid interface value. Consider again the limiting case of small and large permeability ϱ. For large ϱ, the pressure distribution inside the cavity is almost uniformly zero (with very small variation from the tip to the interface), which is indicative of a very slow cavity fluid flow. In contrast, the fluid pressure for small ϱ is characterized by a very steep gradient in the region adjacent to the tip and a significant variation along the cavity. The solution in the small ϱ limit can actually be idealized as a pore fluid flow in the cavity embedded in an impermeable rock (no fluid exchange between the rock and the cavity) from the source located at the tip $\xi = 0$ to the sink located at $\xi = 1$. Comparison of figures 3(b)–5(b) indicates that the range of variation of the pressure in the cavity diminishes with increase in velocity v for a fixed permeability ϱ; this feature of the solution is clearly manifested by the v-dependence of the value of the net-pressure at the fluid interface $\xi = 1$.

The overall characteristics of the cavity solution, namely, the pressure at the fracture tip $\Pi(0)$ and at the fluid interface $\Pi(1)$, and the strength of the effective dipole S (or moment of the source density) are shown on figures 6 and 7, respectively. Figure 6 illustrates further the convergence of the numerical solution towards the large v and small v asymptotic solutions, by showing the pressure at both extremities of the cavity in terms of the two numbers v and η, rather than v and ϱ. It can be seen that the solution for $v = 10^2$ compares very well with the large v asymptote shown in thick dashed lines, whereas the solution for $v = 10^{-3}$ and $v = 10^{-2}$ is practically identical to the small v asymptote shown in thin dashed lines. Similar convergence can be observed in the plot of the dipole strength S versus the parameter η for various fixed values of $v = 10^{-2}, \ldots, 10^2$ (see figure 7). Thus, there is only a narrow range of velocity v where the dipole strength S is appreciably different from both asymptotic solutions. Figure 7 yet again reflects the asymptotic behaviour of the source density at small and large η (or, equivalently, at small and large dimensionless permeability ϱ for a fixed v). Namely, the absolute value of the dipole strength evolves with η
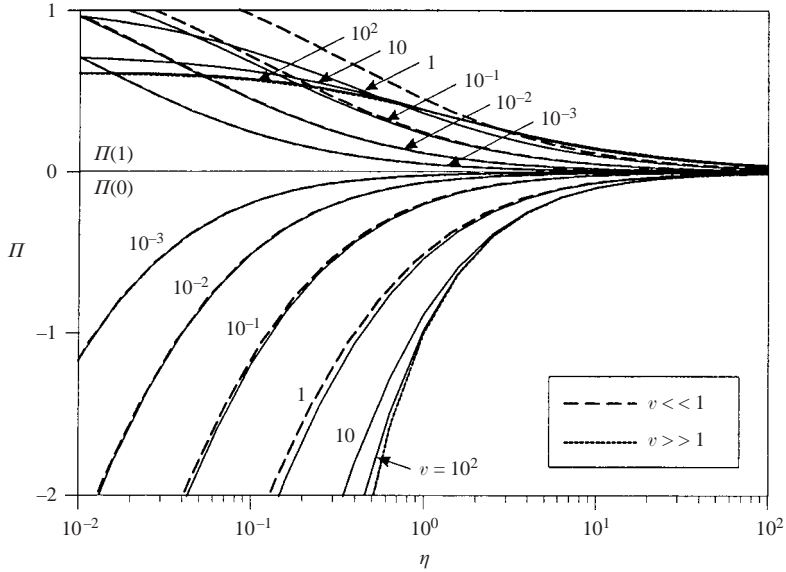
FIGURE 6. Dimensionless fluid pressure Π at the cavity ends ($\xi = 0$ and $\xi = 1$) versus the number $\eta = 4\varrho(v/\pi)^{1/2}$ in a semi-log scale for various values of the dimensionless velocity $v = 10^{-3}, \cdots, 10^2$. The large and small velocity asymptotic solutions for the pressure are shown in thick and thin dashed lines, respectively. (Note that the solution for $v = 10^2$ is indistinguishable from the large velocity solution at $\xi = 1$, whereas solution for $v = 10^{-3}, 10^{-2}$ are practically identical to the small velocity asymptotic solution at both $\xi = 0$ and $\xi = 1$ for the given range of parameter η).
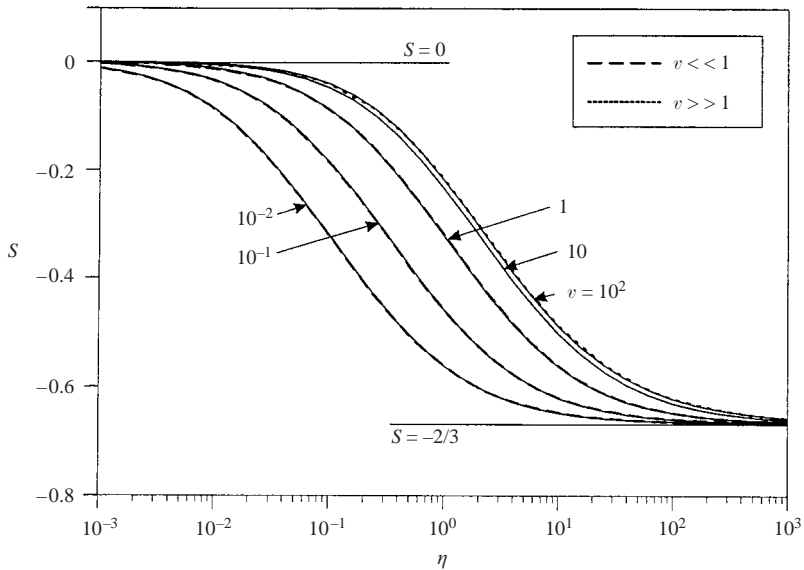

FIGURE 7. Effective dipole strength S (moment of the dimensionless source density γ) versus number $\eta = 4\varrho(v/\pi)^{1/2}$ in a semi-log scale for various values of the dimensionless velocity $v = 10^{-2}, \cdots, 10^2$. The large and small velocity asymptotic solutions are shown by dotted and dashed lines, respectively. (Note that only the solution for $v = 10$ from the given set is significantly different from both asymptotes, whereas the solutions for $v = 10^{-2}, \cdots, 1$ and $v = 10^2$ are practically indistinguishable from the respective asymptotic solutions.)
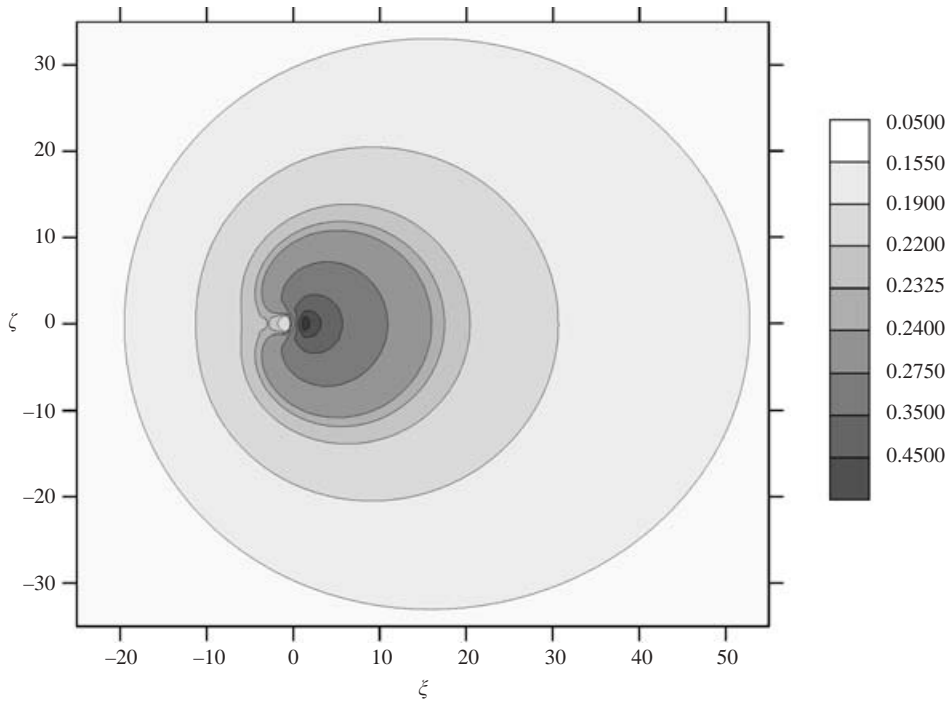
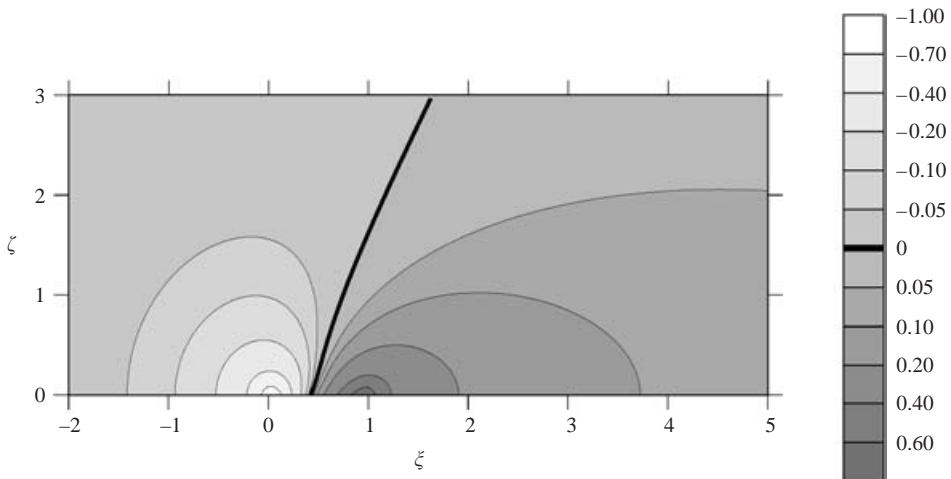FIGURE 8. Pore pressure distribution around the cavity for $v = 0.01$ and $\varrho = 0.1$.

FIGURE 9. Pore pressure distribution around the cavity for $v = 1$ and $\varrho = 0.1$.

(or ϱ) from 0 (no fluid exchange between the cavity and the medium) to 2/3 (maximum exchange).

Contour plots of the pore pressure field around the fracture tip cavity can be seen in figure 8 ($\varrho = 0.1$, $v = 10^{-2}$) and in figure 9 ($\varrho = 0.1$, $v = 1$). The pore pressure field for $v = 10^{-2}$ is shown in figure 8 at a scale large compared to the scale of the cavity; it is like the solution of a moving dipole. (At the scale of the cavity, however, the
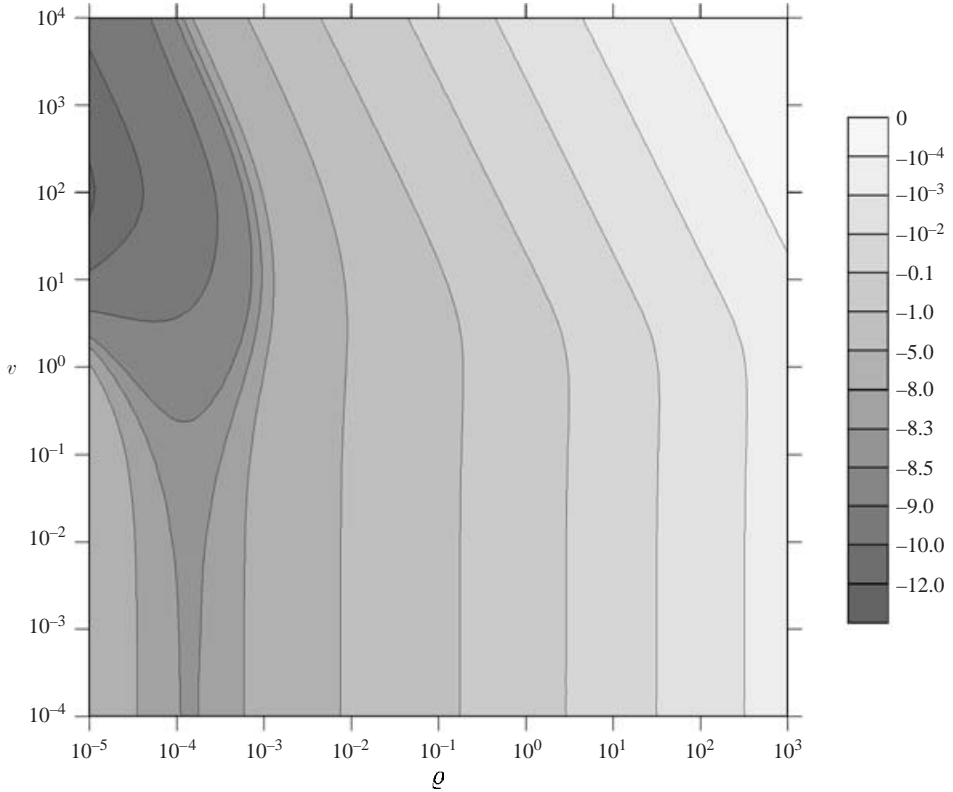
FIGURE 10. Log–log contour plot of the pressure Π at the tip ($\xi = 0$) in the space of parameters ϱ, v.

pore pressure field behaves as a stationary dipole solution.) For the case of moderate velocity ($v = 1$), figure 9 shows that the solution at the cavity scale behaves as a dipole moving in the negative direction along the x-axis.

Finally, contour plots of $\Pi(0)$ and $\Pi(1)$ as a function of ϱ and v are given in figures 10 and 11, respectively. The following conclusions regarding the dependence of $\Pi(0)$ and $\Pi(1)$ on these governing parameters can be drawn from these plots. For a permeability $\varrho \geqslant 10^{-2}$, $\Pi(0)$ and $\Pi(1)$ evolve monotonically with either parameter when the other one is fixed. For example, $\Pi(0)$ ($\Pi(1)$) increases (decreases) monotonically with ϱ when v is fixed, and $\Pi(0)$ ($\Pi(1)$) increases (decreases) monotonically with v when ϱ is fixed. However, $\Pi(0)$ and $\Pi(1)$ have a rather peculiar dependence on the governing parameters ϱ and v, for small $\varrho \leqslant 10^{-2}$. Indeed, when v is fixed and $\varrho \leqslant 10^{-2}$, $\Pi(0)$ as a function of ϱ has a global minimum at $\varrho \sim 10^{-4}$ for small velocity, while it increases monotonically with ϱ for large v. The pressure at the interface $\Pi(1)$ has the opposite behaviour; when v is fixed and $\varrho \leqslant 10^{-2}$, $\Pi(1)$ decreases monotonically with ϱ for small v, while it has a global maximum at $\eta \sim 0.1$ ($\eta \equiv 4\varrho\sqrt{v/\pi}$) for large v. When ϱ is fixed and small ($\varrho \leqslant 10^{-3}$), both $\Pi(0)$ and $\Pi(1)$ have a global minimum at $v \sim 10^{2}$.

One of the interesting features of the $\Pi(1)$ contour plot in the parameter space (ϱ, v) is that it shows the existence of a region where $\Pi(1) < 0$ (around $\varrho \sim 5 \times 10^{-5}$, $v \sim 10^{-2}$). The pore pressure in the vicinity of $\xi \sim 1$ has to be even more negative
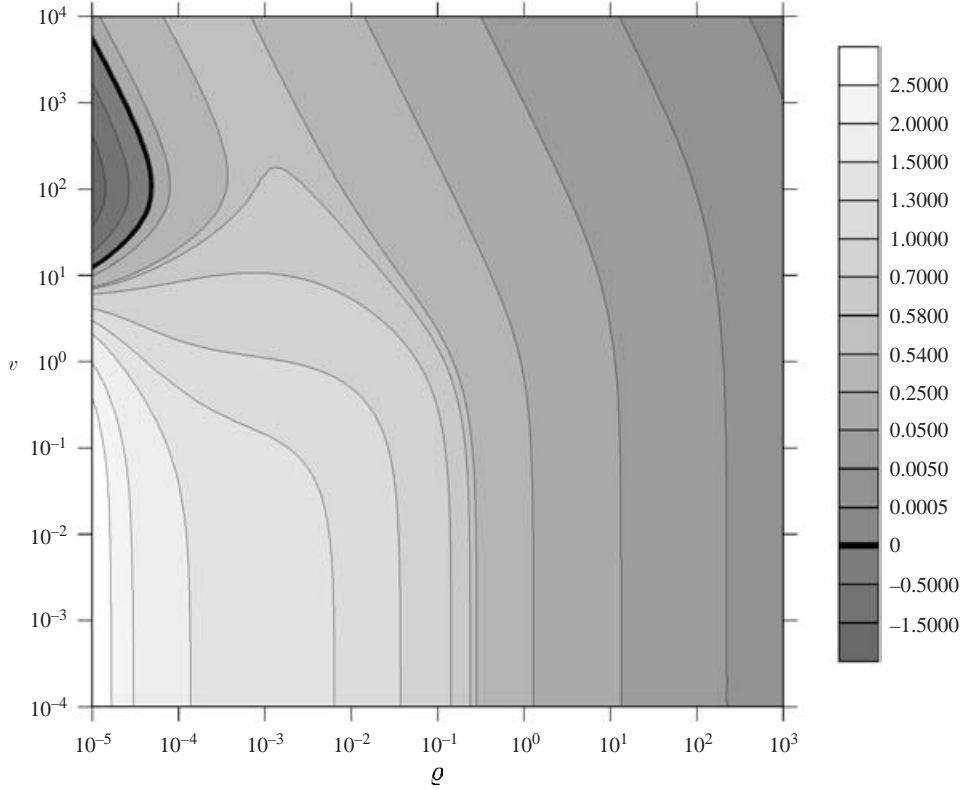
FIGURE 11. Log–log contour plot of the pressure Π at the interface ($\xi = 1$) in the space of parameters ϱ, v.

for the fluid to flow out of the cavity. Hence, there exists a stagnation line, which intersects the tip cavity and which is symmetric with respect to the fracture.

7.2. *Cavitation limit*

The model of fluid flow inside the tip cavity which is described in this paper ceases to be applicable, however, when the fluid cavitates. Let p_c denote the cavitation pressure (the pressure at which fluids vaporize), and Π_c the corresponding dimensionless quantity

$$\Pi_c = \frac{p_c - p_0}{p_*}. \tag{7.1}$$

Since the cavitation pressure p_c is a small negative value, negligible compared either to the confining stress σ_0 or the ambient pore pressure p_0

$$\Pi_c \simeq -\frac{p_0}{p_*} = -\kappa^2 \frac{p_0}{\sigma_0}, \tag{7.2}$$

where κ is the relevant dimensionless toughness for the semi-infinite crack (Garagash & Detournay 2000)

$$\kappa = 2 \left(\frac{\varepsilon \ell_k}{\ell_h} \right)^{1/2} \tag{7.3}$$

with $\ell_h = 12 \mu V / E'$ and $\varepsilon = \sigma_0 / E'$. Furthermore, $\Pi_c \sim -\kappa^2$, since p_0 is usually of the same order of magnitude as σ_0.

Since the fluid pressure is minimum at the fracture tip, the condition for cavitation (if it takes place as the result of a continuous change in the problem parameters) will first be reached at the tip. The cavitation criterion is thus simply

$$\Pi(0) \leqslant \Pi_c. \tag{7.4}$$

Using the condition (7.4), it is straightforward to define the domain in the (ϱ, v) parametric space of figure 10 when cavitation takes place (and the solution discussed in this paper does not hold anymore). Since the dimensionless cavitation pressure Π_c is proportional to κ^2 and since $p_0/\sigma_0 = O(1)$, we can analyse the cavitation phenomenon in terms of κ. According to figure 11, cavitation occurs in the very wide domain in the plane (ϱ, v) to the left of the contour line $\Pi(0) = \Pi_c$ for small toughness κ. As the toughness κ increases, the 'cavitation' domain is pushed to smaller values of the permeability ϱ and with further increase of κ is eventually constrained to very small values of the permeability ϱ and large values of the velocity v (upper left-hand corner in figure 10).

8. Concluding remarks

Modelling the tip of a fluid-driven fracture propagating in a saturated permeable rock involves the description of three coupled processes: fracturing of the rock, fluid flow inside the tip cavity and diffusion of pore fluid in the surrounding porous rock. In this paper, we have been primarily concerned by the calculation of the fluid pressure in the lag region. Hence, we have focused on a particular length scale, the size λ of the tip cavity, out of a sequence of scales which can be described to include (starting from the tip): (i) a process zone, a finite region where the irreversible processes of rock failure linked to fracture propagation are taking place; (ii) a lag region which is filled by pore fluid in the general case of a permeable rock; (iii) a region of rapid change of the fluid pressure; (iv) a region where the fluid pressure is quasi-uniform. This analysis is based on the assumptions that λ is not only large compared to the size of the process zone, but also small compared to the size of the region characterized by a rapid change of the fracturing fluid pressure. The first assumption implies that the tip of the cavity behaves according to the square root asymptote of LEFM; hence, the energy consumed in crack propagation can be subsumed in a single constant, the toughness K_{Ic}. (An additional assumption is, however, involved in adopting $w \sim x^{1/2}$ over the whole tip cavity.) With the second assumption, the problem of the lag region can be analysed as a cavity at the tip of a semi-infinite crack.

One of the main outcomes of this study is the relationship between $\Pi(1)$, the fluid pressure at the interface between the fracturing and the pore fluid, and the length λ of the tip cavity. Another relation between $\Pi(1)$ and λ can, in principle, be obtained from considerations involving the intermediate scale characterized by a rapid change of the fracturing fluid pressure. (Such a relationship was determined for the case of a hydraulic fracture propagating in an impermeable medium by Garagash & Detournay 2000). The knowledge of both λ and $\Pi(1)$ provides the pressure boundary condition for the flow of fracturing fluid in the fracture and, therefore, is the key for constructing the overall solution of a hydraulic fracture propagating in a permeable rock. Finally, the fluid pressure at the tip of the crack, $\Pi(0)$, can be used to calculate the conditions at which cavitation takes place, which marks the breakdown of this solution.

this work by the Graduate School of the University of Minnesota in the form of a Doctoral Research Fellowship (1997–1998).

Appendix A. Small velocity asymptotic case
A.1. *Inversion of Cauchy singular integral equation*

This Appendix outlines the inversion of the Cauchy singular integral equation (4.3) to obtain an integral expression $\Upsilon(\xi)$ as a function of $\Pi(\xi)$ that satisfies the boundary conditions (4.4). Following Muskhelishvili (1977), we introduce the complex function

$$\Phi(z) = \frac{1}{2\pi i} \int_0^1 \frac{\Upsilon(u)\, du}{u - z}, \tag{A 1}$$

where z is a complex variable and $\Upsilon(\xi)$ is assumed to satisfy the Holder condition on the interval $\xi \in [0, 1]$. The function $\Phi(z)$ is analytic in the complex plane with a branch cut along the interval $[0, 1]$ of the real axis. According to the Plemelj formulae and (4.3),

$$\Phi^+(\xi) - \Phi^-(\xi) = \Upsilon(\xi), \tag{A 2}$$

$$\Phi^+(\xi) + \Phi^-(\xi) = \frac{1}{\pi i} \int_0^1 \frac{\Upsilon(u)\, du}{u - \xi} = \frac{2\varrho}{i} \Pi(\xi), \tag{A 3}$$

where $\xi \in [0, 1]$ and $\Phi^\pm(\xi) = \Phi(\xi \pm i0)$ are the limiting values of $\Phi(z)$ on the interval $z \in [0, 1]$ approached from positive and negative imaginary z, respectively. Whereas (A 2) provides the solution for $\Upsilon(\xi)$ once $\Phi(z)$ is found, (A 3) defines a Hilbert boundary value problem with general solution given by

$$\Phi(z) = -\frac{\varrho X(z)}{\pi} \int_0^1 \frac{\Pi(u)\, du}{X^+(u)(u - z)} + X(z)Q(z). \tag{A 4}$$

In the above, $X(z)$ is the solution of the homogeneous Hilbert problem ($\Phi^+(\xi) + \Phi^-(\xi) = 0$, $\xi \in [0, 1]$) and $Q(z)$ is an arbitrary polynomial. Since $\Upsilon(\xi)$ is bounded at the endpoints ($\Upsilon(0) = \Upsilon(1) = 0$), $\Phi(z)$ is also bounded at $z = 0$ and at $z = 1$. Hence, out of four possible solutions, $X(z)$ is given by

$$X(z) = C\, z^{1/2}(1 - z)^{1/2}, \tag{A 5}$$

where C is an arbitrary constant. The function $\Upsilon(\xi)$ is then deduced from (A 4) and (A 2)

$$\Upsilon(\xi) = -\frac{2\varrho}{\pi} \xi^{1/2}(1 - \xi)^{1/2} \int_0^1 \frac{\Pi(u)}{u^{1/2}(1 - u)^{1/2}} \frac{du}{u - \xi} + \xi^{1/2}(1 - \xi)^{1/2} Q(\xi). \tag{A 6}$$

Equation (4.3) provides an expression for the dimensionless pressure $\Pi(\xi)$ along the ξ-axis ($\eta = 0$), not only in the cavity $\xi \in [0, 1]$, but outside the cavity as well, provided that $\xi < 1/v$ (corresponding to the range of validity of (4.3)). Since, the pressure at infinity ($\xi \to \infty$) must approach the far-field value, the integral in (4.3) must converge for $\xi \to \infty$. This is possible only if the second term in (A 6) is absent. Consequently, $Q(\xi)$ must be taken to zero in (A 6).

A.2. *Sine series expansion of the kernel $K(\xi, u)$*

Consider the transformation of coordinates $\xi = \cos^2 \varphi$, $u = \cos^2 \theta$. The kernel $K(\xi, u)$, given by (4.8), then transforms as

$$K(\cos^2 \varphi, \cos^2 \theta) = \bar{K}(\varphi, \theta) = \bar{K}_1 + \bar{K}_2, \tag{A 7}$$

where

$$\bar{K}_1 = \ln \left| \frac{\cos\theta + \cos\varphi}{\cos\theta - \cos\varphi} \right|, \qquad \bar{K}_2 = \ln \left| \frac{1 - \cos(\theta + \varphi)}{1 + \cos(\theta - \varphi)} \right|. \tag{A 8}$$

The following Fourier series (Porter & Stirling 1990) hold

$$\bar{K}_1 = \sum_{n=1}^{\infty} \frac{4}{2n-1} \cos[(2n-1)\varphi] \cos[(2n-1)\theta], \tag{A 9}$$

$$\tfrac{1}{2} \ln[2(1 - \cos\omega)] = -\sum_{n=1}^{\infty} \frac{1}{n} \cos n\omega. \tag{A 10}$$

Thus, from (A 8) and (A 10),

$$\bar{K}_2 = \sum_{n=1}^{\infty} \frac{2}{n}((-1)^n \cos[n(\theta - \varphi)] - \cos[n(\theta + \varphi)])$$

$$= -\sum_{k=1}^{\infty} \frac{4}{2k-1} \cos[(2k-1)\varphi] \cos[(2k-1)\theta] + \sum_{k=1}^{\infty} \frac{2}{k} \sin(2k\varphi) \sin(2k\theta). \tag{A 11}$$

According to (A 7), (A 9) and (A 11), the kernel $\bar{K}(\varphi, \theta)$ can then be expressed as a double sine Fourier series

$$\bar{K}(\varphi, \theta) = \sum_{k=1}^{\infty} \frac{2}{k} \sin(2k\varphi) \sin(2k\theta). \tag{A 12}$$

Appendix B. Large velocity asymptotic case

We consider the integral equation (2.28) for the large dimensionless velocity $v \gg 1$

$$I(\xi; v, \varrho) = \Pi(\xi), \tag{B 1}$$

where $I(\xi; v, \varrho)$ denotes the convolutional integral

$$I(\xi; v, \varrho) = \frac{1}{2\pi\varrho} \int_0^1 \gamma(u) \exp\left[\frac{v(\xi - u)}{2}\right] K_0\left(\frac{v|\xi - u|}{2}\right) du. \tag{B 2}$$

The asymptotic expression of $I(\xi; v, \varrho)$ for large v is based on approximating the modified Bessel function $K_0(\zeta)$ for $\zeta > \zeta_0$, where $\zeta_0 = O(1)$, by the first term of its asymptotic expansion for large arguments (Abramowitz & Stegun 1964)

$$K_0(\zeta) \sim \left(\frac{\pi}{2\zeta}\right)^{1/2} e^{-\zeta}, \quad \zeta > \zeta_0. \tag{B 3}$$

The integral $I(\xi)$ in (B 2) is then written as the sum of three integrals

$$I = I_- + I_0 + I_+, \tag{B 4}$$

where I_-, I_0 and I_+ denote the integrals over the subintervals $[0, \xi - \epsilon]$, $[\xi - \epsilon, \xi + \epsilon]$ and $[\xi + \epsilon, 1]$, respectively; ϵ is a small number defined as $\epsilon = 2\zeta_0/v$.

If ξ is a inner point of the $(0, 1)$ interval and if γ is regular function at ξ, the integral $I_0(\xi)$ can be approximated as

$$I_0(\xi) \simeq \frac{\gamma(\xi)}{\pi\varrho v} \int_{-\zeta_0}^{\zeta_0} e^\zeta K_0(|\zeta|) \, d\zeta = \frac{2\zeta_0}{\pi\varrho v} [K_0(\zeta_0) \cosh\zeta_0 + K_1(\zeta_0) \sinh\zeta_0] \gamma(\xi), \tag{B 5}$$

while the integral $I_-(\xi)$ and an upper bound of $|I_+(\xi)|$ can be estimated using the asymptotic expression (B 3)

$$I_-(\xi) \simeq \frac{1}{2\varrho(\pi v)^{1/2}} \int_0^{\xi-\epsilon} \frac{\gamma(u)}{(\xi-u)^{1/2}}\, \mathrm{d}u \simeq \frac{1}{2\varrho(\pi v)^{1/2}} \int_0^{\xi} \frac{\gamma(u)}{(\xi-u)^{1/2}}\, \mathrm{d}u, \qquad (\text{B 6})$$

$$|I_+(\xi)| \leqslant \frac{\gamma_m}{\varrho v(2\pi)^{1/2}} \int_{\zeta_0}^{v(1-\xi)/2} \frac{\mathrm{e}^{-2\zeta}}{\zeta^{1/2}}\, \mathrm{d}\zeta = \frac{\gamma_m}{2\varrho v} \left[\mathrm{erf}(v(1-\xi))^{1/2} - \mathrm{erf}(2\zeta_0)^{1/2}\right]. \quad (\text{B 7})$$

Hence,

$$|I_+(\xi)| < \frac{\gamma_m}{2\varrho v}, \qquad (\text{B 8})$$

where $\gamma_m = \max |\gamma(u)|$ on the interval $u \in (\xi, 1)$.

If γ is singular at $\xi = 1$, let $\xi_* \in (\xi, 1)$ be such that $\gamma(u) = O(1)$ for $u \in (\xi, \xi_*)$. After splitting the integral I_+ over the two subintervals (ξ, ξ_*) and $(\xi_*, 1)$, an upper bound of $|I_+|$ is then given by

$$|I_+| \leqslant \frac{\gamma_*}{\varrho v(2\pi)^{1/2}} \int_{\zeta_0}^{v(\xi_*-\xi)/2} \frac{\mathrm{e}^{-2\zeta}}{\zeta^{1/2}}\, \mathrm{d}\zeta + \frac{|\Upsilon(\xi_*)|}{\varrho v^{3/2}} \frac{\mathrm{e}^{-v(\xi_*-\xi)}}{[\pi(\xi_*-\xi)]^{1/2}}, \qquad (\text{B 9})$$

where $\gamma_* = \max |\gamma(u)|$ on the interval $u \in (\xi, \xi_*)$. Also, $|\Upsilon(\xi_*)|$ represents the total fluid volume exchanged between the porous medium and the cavity over the interval $(\xi_*, 1)$ and must therefore be finite. Hence, the second term in the sum (B 9) is exponentially small and the order of I_+ is given by the first term.

In summary, the dependence of the integrals on v are: $I_- = O(1/v^{1/2})$, $I_0, I_+ = O(1/v)$. Only the leading term I_- therefore needs to be retained in the integral (B 4) at large v; hence,

$$I(\xi) \simeq \frac{1}{2\varrho(\pi v)^{1/2}} \int_0^{\xi} \frac{\gamma(u)\, \mathrm{d}u}{(\xi-u)^{1/2}}. \qquad (\text{B 10})$$

It follows that the integral equation (B 2) takes the form

$$\frac{2}{\pi} \int_0^{\xi} \frac{\gamma(u)\, \mathrm{d}u}{(\xi-u)^{1/2}} = \eta \Pi(\xi), \qquad (\text{B 11})$$

where

$$\eta = 4\varrho \left(\frac{v}{\pi}\right)^{1/2}. \qquad (\text{B 12})$$

Appendix C. Numerical algorithm for the tip cavity solution

The numerical procedure for solving the integral equation (6.4) with the constraint (6.6) in terms of the 'regularized' source density γ_r and the tip pressure $\Pi(0)$ is outlined here. The integration interval $\xi \in [0, 1]$ is divided into N contiguous elements (a_j, a_{j+1}), $j = 1, \dots, N$ with $a_1 = 0$ and $a_{N+1} = 1$. Let ξ_j, $j = 1, \dots, N$ denote the midpoints of these segments. The source density $\gamma_r(\xi)$ is then defined as a piecewise constant function over these elements

$$\gamma_r(\xi) = \begin{cases} \gamma_j & \text{if } \xi \in (a_j, a_{j+1}), \\ 0 & \text{elsewhere.} \end{cases} \qquad (\text{C 1})$$

The expression (6.3) for the pressure in terms of the source density evaluated at the midpoint ξ_i of the ith element takes the form

$$\Pi^i = \Pi(0) + \sum_{j=1}^{N} \phi_{ij}^p \gamma_j, \tag{C 2}$$

where

$$\phi_{ij}^p = 2\left[-\xi_i^{-1/2}(a_{j+1} - a_j) + 2\left(a_{j+1}^{1/2} - a_j^{1/2}\right)\right] D_{ij}$$
$$+ 2\left[-\xi_i^{-1/2}(\xi_i - a_i) + 2\left(\xi_i^{1/2} - a_i^{1/2}\right)\right]\delta_{ij}. \tag{C 3}$$

In (C3), δ_{ij} is the Kronecker-delta and D_{ij} is defined as $D_{ij} = 1$ if $j < i$, and $D_{ij} = 0$ if $j \geqslant i$.

Substituting (C 1) into (6.4) and (6.6) and selecting the element midpoints as collocation points (while taking into account (C 2)) yields the following system of $N + 1$ linear equation to be solved for the $N + 1$ unknowns γ_j, $j = 1, \ldots, N$, and $\Pi(0)$

$$\left.\begin{aligned} \Pi(0) + \sum_{j=1}^{N} \left(\phi_{ij}^p - \phi_{ij}\right)\gamma_j &= \Pi_t^i, \\ \sum_{j=1}^{N} (a_{j+1} - a_j)\gamma_j &= 1, \end{aligned}\right\} \tag{C 4}$$

where $\Pi_t^i = \Pi_t(\xi_i)$ and

$$\phi_{ij} = \int_{a_j}^{a_{j+1}} \Pi_s(\xi_i - u, 0)\, \mathrm{d}u = -(\pi\varrho v)^{-1}[f(b_{i\,j+1}) - f(b_{ij})], \qquad b_{ij} = \tfrac{1}{2}v(\xi_i - a_j),$$
$$\tag{C 5}$$

The function f in (C 5) is expressed in terms of the modified Bessel functions of the second kind, K_0 and K_1

$$f(\xi) = \int^{\xi} \exp(u)K_0(|u|)\, \mathrm{d}u = \exp(\xi)[\xi K_0(|\xi|) + |\xi|K_1(|\xi|)].$$

After solving the linear system of equations (C 4) for the γ_i terms and $\Pi(0)$, the nodal pressure Π^i terms are calculated from (C 2).

REFERENCES

ABÉ, H., MURA, T. & KEER, L. M. 1976 Growth rate of a penny-shaped crack in hydraulic fracturing of rocks. *J. Geophys. Res.* **81**, 5335–5340.

ABRAMOWITZ, M. & STEGUN, I. A. (ed.) 1964 *Handbook of Mathematical Functions with Formulas, Graphs, and Mathematical Tables*. US Govt Printing Office, Washington, DC.

ADACHI, J., DETOURNAY, E. & CARBONELL, R. 2003 Plane strain propagation of a hydraulic fracture II: zero-toughness self-similar solution. *Proc. R. Soc. Lond.* A (To be submitted).

ADACHI, J. I. & DETOURNAY, E. 2002 Self-similar solution of a plane-strain fracture driven by a power-law fluid. *Intl J. Numer. Anal. Meth. Geomech.* **26**, 579–604.

BARENBLATT, G. 1962 The mathematical theory of equilibrium cracks in brittle fracture. *Adv. Appl. Mech.* **7**, 55–129.

BATCHELOR, G. K. 1967 *An Introduction to Fluid Dynamics*. Cambridge University Press.

BEAR, J. 1988 *Dynamics of Fluids in Porous Media*. Dover.

BIOT, M. 1941 General theory of three-dimensional consolidation. *J. Appl. Phys.* **12**, 155–164.

CARBONELL, R., DESROCHES, J. & DETOURNAY, E. 1999 A comparison between a semi-analytical and a numerical solution of a two-dimensional hydraulic fracture. *Intl J. Solids Struct.* **36** (31–32), 4869–4888.

CARSLAW, H. & JAEGER, J. C. 1959 *Conduction of Heat in Solids*, 2nd edn. Oxford University Press.

DESROCHES, J., DETOURNAY, E., LENOACH, B., PAPANASTASIOU, P., PEARSON, J. R. A., THIERCELIN, M. & CHENG, A. H.-D. 1994 The crack tip region in hydraulic fracturing. *Proc. R. Soc. Lond.* A **447**, 39–48.

DETOURNAY, E., ADACHI, J. I. & GARAGASH, D. I. 2002 Asymptotic and intermediate asymptotic behavior near the tip of a fluid-driven fracture propagating in a permeable elastic medium. In *Structural Integrity and Fracture* (ed. A. V. Dyskin, X. Hu & E. Sahouryeh), pp. 9–18. Balkema.

DETOURNAY, E. & CHENG, A.-D. 1993 Fundamentals of Poroelasticity. *Comprehensive Rock Engineering*, vol. 2, chap. 5, pp. 113–171. Pergamon.

DETOURNAY, E., CHENG, A.-D. & MCLENNAN, J. 1990 A poroelastic PKN hydraulic fracture model based on an explicit moving mesh algorithm. *Trans. ASME: J. Energy Resour. Technol.* **112**, 224–230.

GARAGASH, D. I. 2000 Hydraulic fracture propagation in elastic rock with large toughness. In *Rock Around the Rim – Proc. 4th North American Rock Mechanics Symp.* (ed. J. Girard, M. Liebman, C. Breeds & T. Doe), pp. 221–228. Balkema.

GARAGASH, D. I. & DETOURNAY, E. 2002 Viscosity-dominated regime of a fluid-driven fracture in an elastic medium. In *IUTAM Symp. on Analytical and Computational Fracture Mechanics of Non-Homogeneous Materials* (ed. B. L. Karihaloo). Kluwer.

GARAGASH, D. I. & DETOURNAY, E. 2000 The tip region of a fluid-driven fracture in an elastic medium. *Trans. ASME: J. Appl. Mech.* **67**, 183–192.

GEERTSMA, J. & HAAFKENS, R. 1979 A comparison of the theories for predicting width and extent of vertical hydraulically induced fractures. *Trans. ASME: J. Energy Resour. Technol.* **101**, 8–19.

GEERTSMA, J. & DE KLERK, F. 1969 A rapid method of predicting width and extent of hydraulic induced fractures. *J. Petrol. Tech.* **246**, 1571–1581 (SPE 2458).

GORDEYEV, Y. 1993 Growth of a crack produced by hydraulic fracture in a poroelastic medium. *Intl J. Rock Mech. Min. Sci.* **30**, 233–238.

GRIFFITH, A. 1921 The phenomena of rupture and flow in solids. *Phil. Trans. R. Soc. Lond.* A **221**, 163–197.

IRWIN, G. 1957 Analysis of stresses and strains near the end of a crack traversing a plate. *Trans. ASME: J. Appl. Mech.* **24**, 361–364.

KEVORKIAN, J. & COLE, J. 1996 *Multiple Scale and Singular Perturbation Methods*. Springer.

KHRISTIANOVIC, S. & ZHELTOV, Y. 1955 Formation of vertical fractures by means of highly viscous fluids. In *Proc. 4th World Petroleum Congress, Rome*, vol. 2, pp. 579–586.

LENOACH, B. 1995 The crack tip solution for hydraulic fracturing in a permeable solid. *J. Mech. Phys. Solids* **43**, 1025–1043.

LISTER, J. R. 1990 Buoyancy-driven fluid fracture: the effects of material toughness and of low-viscosity precursors. *J. Fluid Mech.* **210**, 263–280.

MUSKHELISHVILI, N. 1977 *Singular Integral Equations*. Noordhoff.

NILSON, R. 1988 Similarity solutions for wedge-shaped hydraulic fracture driven into a permeable medium by a constant inlet pressure. *Intl J. Numer. Anal. Meth. Geomech.* **12**, 477–495.

NORDGREN, R. 1972 Propagation of vertical hydraulic fractures. *J. Petrol. Technol.* **253**, 306–314, (SPE 3009).

PAPANASTASIOU, P. 1997 The influence of plasticity in hydraulic fracturing. *Intl J. Fracture* **84**, 61–97.

PERKINS, T. K. & KERN, L. R. 1961 Widths of hydraulic fractures. *J. Petrol. Technol., Trans. AIME* **222**, 937–949.

PORTER, D. & STIRLING, D. 1990 *Integral Equations: A Practical Treatment, from Spectral Theory to Applications*. Cambridge University Press.

RICE, J. R. & CLEARY, M. 1976 Some basic stress-diffusion solutions for fluid saturated elastic porous media with compressible constituents. *Rev. Geophys. Space Phys.* **14**, 227–241.

RICE, J. R. 1968 Mathematical analysis in the mechanics of fracture. In *Fracture, an Advanced Treatise* (ed. H. Liebowitz), vol. 2, chap. 3, pp. 191–311. Academic.

RUBIN, A. M. 1993 Tensile fracture of rock at high confining pressure: Implications for dike propagation. *J. Geophys. Res.* **98** (B9), 15 919–15 935.

RUBIN, A. M. 1995 Propagation of magma-filled cracks. *Annu. Rev. Earth Planet. Sci.* **23**, 287–336.

SAVITSKI, A. A. & DETOURNAY, E. 2002 Propagation of a fluid-driven penny-shaped fracture in an impermeable rock: asymptotic solutions. *Intl J. Solids Struct.* **39** (26), 6311–6337.

SPENCE, D. A. & TURCOTTE, D. 1985 Magma-driven propagation crack. *J. Geophys. Res.* **90**, 575–580.

SPENCE, D. A. & SHARP, P. W. 1985 Self-similar solution for elastohydrodynamic cavity flow. *Proc. R. Soc. Lond.* A **400**, 289–313.

ZAZOVSKYI, A. & PANKO, S. 1978 Local structure of the solution of the associated problem of a hydraulic fault crack in a permeable medium. *Izv. Akad. Nauk. SSSR. Mekh. Tverdogo Tela* **13** (5), 153–158.